The Energetics and Reversibility of Oxyanions Adsorption/ Desorption on Pure and Aluminium-Substituted Ferrihydrite

THE ENERGETICS AND REVERSIBILITY OF OXYANIONS ADSORPTION/DESORPTION ON PURE AND ALUMINIUM-SUBSTITUTED FERRIHYDRITE

by

ALIREZA NAMAYANDEH

Under the Direction of Nadine Kabengi, PhD

ABSTRACT

This work examines the adsorption, desorption, and reversibility of five oxyanions (chloride, nitrate, sulfate, phosphate and arsenate) with ferrihydrite (Fh) using mostly thermodynamics data acquired from flow microcalorimetry. In addition, the role of aluminum incorporation on the physical and chemical properties of Fh is investigated. The adsorption of phosphate, sulfate, arsenate, chloride, and nitrate by Fh was examined at pH 5.6, and the enthalpy of interaction (ΔH) was found to follow a positive Hofmeister series such as ($\Delta H_{Cl^-} = \Delta H_{NO_3^-} < \Delta H_{SO_4^{2-}} < \Delta H_{PO_4^-} < \Delta H_{AsO_4^{2-}}$). The ΔH values and reversibility of adsorption mirrored their modes of surface complexation. The adsorption/desorption and reversibility of sulfate on three Fh samples precipitated with 0, 12 and 24 mol % Al were examined at both pH 5.6 and 3.0. Results show an increase in the heat of exchange, irreversibility, and a fraction of inner-sphere complexes with increasing Al concentration and decreasing pH values.

INDEX WORDS: Oxyanion adsorption, Calorimetry, Sulfate, Aluminum substitution, reversibility, Anion exchange

THE ENERGETICS AND REVERSIBILITY OF OXYANIONS ADSORPTION/DESORPTION ON PURE AND ALUMINIUM-SUBSTITUTED FERRIHYDRITE

by

ALIREZA NAMAYANDEH

A Thesis Submitted in Partial Fulfillment of the Requirements for the Degree of

Master of Science, Chemistry

in the College of Arts and Sciences

Georgia State University

2018

THE ENERGETICS AND REVERSIBILITY OF OXYANIONS ADSORPTION/DESORPTION ON PURE AND ALUMINIUM-SUBSTITUTED FERRIHYDRITE

by

ALIREZA NAMAYANDEH

Committee Chair: Nadine Kabengi

Committee: Kathryn Grant

Michael L. Machesky

Electronic Version Approved:

Office of Graduate Studies

College of Arts and Sciences

Georgia State University

August 2018

DEDICATION

To Shagahyegh Navabpour

ACKNOWLEDGMENTS

I thank my family and friends for unwavering support and love. I would also like to thank my advisor, Dr. Nadine Kabengi, for offering her knowledge and guidance and also all the members of her group who helped me during my studies.

The SSA and electron microscopy work were supported by the Virginia Tech National Center for Earth and Environmental Nanotechnology Infrastructure (NanoEarth), a member of the National Nanotechnology Coordinated Infrastructure (NNCI), supported by NSF (ECCS 1542100). I would also like to thank Mrs. Deborah Berti and Dr. Weinan Leng from NanoEarth.

The zeta potential measurement was conducted in Daniel Environmental Engineering Laboratory in Georgia Tech University. Special thanks to Dr. Yongsheng Chen and his Ph.D. student Bopeng Zhang who helped me with their lab's facilities.

I also would like to thank Dr. Daniel Deocampo and Dr. Crawford Elliott for helping to run my samples on the X-ray diffractometer and David Davis who assisted me during the analysis.

Not to be forgotten is Professor Michael Hochella who helped me to get this opportunity and has generously given me his advice and kind support over the past five years.

TABLE OF CONTENTS

ACKNOWLEDGMENTS .... **II**

LIST OF TABLES .... **VII**

LIST OF FIGURES .... **VIII**

LIST OF ABBREVIATIONS .... **IX**

1 INTRODUCTION **1**

1.1 Adsorption **1**

1.2 Ferrihydrite Structure **1**

1.3 Aluminum Substituted Fh **3**

1.4 Oxyanions **4**

1.5 Overview **6**

2 THE ENERGETICS OF OXYANION SORPTION ON FERRIHYDRITE STUDIED USING FLOW MICROCALORIMETRY **7**

2.1 Introduction **7**

2.2 Materials and Methods **9**

2.2.1 Chemicals ***9***

2.2.2 ***Characterization*** ***10***

2.2.3 Experiments ***12***

2.3 Results and Discussion **13**

2.3.1 Energetics of Exchange and Adsorption *13*

2.3.2 Desorption and Reversibility *17*

2.4 Conclusion **19**

3 THE ROLE OF ALUMINUM SUBSTITUTION INTO FERRIHYDRITE ON THE MECHANISMS OF THE SULFATE ADSORPTION/DESORPTION. **20**

3.1 Introduction **20**

3.2 Materials and Methods **23**

3.2.1 Mineral Synthesis *23*

3.2.2 Sample Characterization *23*

3.2.3 Calorimetric Measurements *24*

3.3 Results **27**

3.3.1 *Characterization* *27*

3.3.2 Chloride and Nitrate Exchange: Pre-Sulfate Treatment *27*

3.3.3 Sulfate Sorption *29*

3.3.4 Chloride and Nitrate Exchange: Post-Sulfate Treatment *32*

3.4 DISCUSSION **35**

3.4.1 Surface Charge *35*

3.4.2 Sulfate Adsorption *36*

3.4.3 Sulfate Desorption and Reversibility *37*

3.5 Conclusion **40**

4 CONCLUSIONS **42**

4.1 Future Work **44**

REFERENCES **46**

APPENDICES **54**

Appendix A **54**

Appendix A.1. Oxyanion specific properties ***54***

Appendix B **55**

Appendix B.2. Representative X-ray Diffraction Pattern for Ferrihydrite ***55***

Appendix B.3. Representative High-Resolution Transmission Electron Micrograph of the Ferrihydrite Sample ***55***

Appendix B.4. Instrumentation and Basic Operational Procedure for the Flow Microcalorimeter ***56***

Appendix B.5. a) Peaks Obtained From a Series of Heat Pulses, and b) The Associated Calibration Curve. ***57***

Appendix C **58**

Appendix C.1. Representative X-ray Diffraction Pattern for Different Aluminum Ferrihydrite ***58***

Appendix C.2. Zeta Potential Data for Ferrihydrite (0AlFh), and Al-ferrihydrite (12AlFh and 24AlFh) ***58***

Appendix C.3. Transmission Electron Micrographs and Energy Dispersive X-ray Spectroscopy Analysis of Different Aluminum Ferrihydrite ***59***

Appendix C.4. The Q_{exch} of C/N (mJ/mg) of Various AlFh at pH 5.6 and pH 3.... 60

LIST OF TABLES

Table 2.1. Experimental conditions for the adsorption experiments. 10

Table 2.2. The speciation of the oxyanions under the experimental conditions........................... 11

Table 2.3. Summary of the heat of exchange values corresponding to the adsorption of oxyanions. 15

Table 2.4. The heat of exchange for the representative pretreatment [C/N], the first posttreatment [C/N] and the equilibrium posttreatment. 18

Table 3.1. A summary of the physical and chemical properties of the samples........................... 28

Table 3.2. The heat of exchange for the representative pretreatment [C/N], the first posttreatment [C/N] 29

Table 3.3. The heat of adsorption and enthalpy of sulfate adsorption on various AlFh and pHs. 31

Table 3.4. The heat of exchange for the representative pretreatment [C/N], the equilibrium posttreatment and the volume of solution used to reach the equilibrium posttreatment 34

LIST OF FIGURES

Figure 1.1. *The basic structural motif of the ideal ferrihydrite structure. The central FeO_4 tetrahedra are surrounded by 12 FeO_6 octahedra (Michel et al 2007)*... 2

Figure 1.2. Keggin moiety of the ideal ferrihydrite structure (Heimestra 2013)........................... 3

Figure 2-1. The calorimetric signal for a) chloride and nitrate exchange, b) sulfate adsorption and c) phosphate and arsenate adsorption. 14

Figure 3.1. The calorimetric signals for chloride and nitrate exchange for 0AlFh, 12 AlFh, and 24AlFh at a) pH 5.6 and b) pH 3. 28

Figure 3-2. The calorimetric signal for sulfate adsorption for 0AlFh, 12 AlFh, and 24AlFh at a) pH 5.6and b) pH 3. 30

Figure 3-3. Representative calorimetric signals for [C/N] and [N/C] cycles before and after sulfate treatment.. 33

Figure 3.4. Qualitative estimation of the variation in reversibility of sulfate desorption with Al concentration and pH.. 39

LIST OF ABBREVIATIONS

FAMC	Flow Adsorption Microcalorimetry
ΔH_{ads}	Enthalpy of Adsorption
HRTEM	High-Resolution Transmission Electron Microscopy
BET	Brunauer–Emmett–Teller
Q_{ads}	Heat of Adsorption
ICP-OES	Inductively Coupled Plasma Optical Emission Spectroscopy
PDF	X-ray Pair Distribution Function analysis
Fh	Ferrihydrite
XRD	X-ray Diffraction
[C/N]	Nitrate Replacing Chloride
[N/C]	Chloride Replacing Nitrate
[C/S]	Sulfate Replacing Chloride
[S/C]	Chloride Replacing Sulfate
[C/P]	Phosphate Replacing Chloride
[C/AS]	Arsenate Replacing Chloride
PZC	Point of Zero Charge
EXAFS	X-ray Absorption Fine Structure
SCM	Surface Complexation Modeling
SSA	Specific Surface Area
EDS	Energy Dispersive X-ray Spectroscopy
AlFh	Aluminum Ferrihydrite

1 INTRODUCTION

1.1 Adsorption

Adsorption is a critical mechanism by which natural and anthropogenic contaminants are transported in aquatic and terrestrial systems [1-4]. The extent to which adsorption mechanisms control the fate and transport of contaminants depends on the chemistries of the aqueous phase and the nature, size, and reactivity of the mineral surfaces present [1-5]. Because of their relatively high specific surface areas and reactivity, iron oxides and oxyhydroxides are some of the most important minerals controlling the adsorption of contaminants. Iron hydroxides are ubiquitous in nature existing as relatively pure minerals such as goethite (Goe; α-FeOOH)) and hematite (Hm; α-Fe_2O_3), and as ferrihydrite (Fh; $Fe_{10}O_{15}$ $9H_2O$), a poorly crystallized hydrous phase which is arguably the most pervasive and relevant phase in different surface environments. [3, 5-8].

1.2 Ferrihydrite Structure

Fh occurs in soils and sediments where it occurs both naturally and as a result of anthropogenic activities such as acid mine drainage. It's *in situ* precipitation creates nanoparticles (1–3 nm in size) of very high specific surface areas, for which values as high as ~1250 m^2/g have been reported [9-12].

Recently, there has been focused attention on the structure of Fh. In the past, several standard models have been suggested for the structure of Fh [13-14]. Drits et al. [15] formulated the standard model for the structure of Fh which was the most acceptable model until recently. This model includes three intermingled phases composed of octahedrally coordinated Fe with variable stacking sequences of the iron octahedra. In 2007, Michel et al. [9] overturned this model by proposing a new crystal structure for Fh based on one phase, the isostructural akdalaite ($Al_{10}O_{14}(OH)_2$). These researchers using synchrotron X-ray Pair Distribution Function analysis

(PDF) found that besides having Fe in hexacoordination, Fh contains Fe in tetrahedral coordination as well. Based on the ideal form of this structure, $Fe_{10}O_{14}(OH)_2$ has been suggested as the chemical formula for Fh [9]. Figure 1.1 shows the basic structural motif of the model which comprises 13 iron atoms and 40 oxygens. As seen, there is a central tetrahedrally coordinated Fe attached to 12 outer octahedrally coordinated Fe atoms [9]. Accordingly, three types of Fe sites have been considered for the ideal structure of Fh. Fe1 and Fe2 are hexa-coordinated and occupy 60% and 20% of the structure, respectively, whereas Fe is tetrahedrally coordinated and occupies 20% of the structure. In Figure 2, the tetrahedrally coordinated Fe (Fe) can be observed in the center of a δ-Keggin moiety as a part of the Fh structure [11, 16].

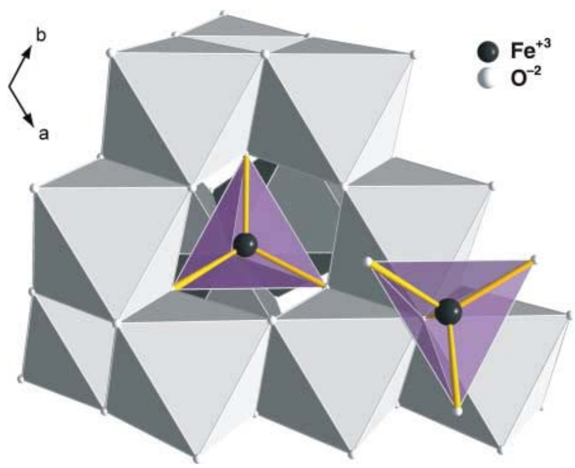

Figure 1.1. *The basic structural motif of the ideal ferrihydrite structure. The central FeO_4 tetrahedra are surrounded by 12 FeO_6 octahedra (Michel et al 2007)*

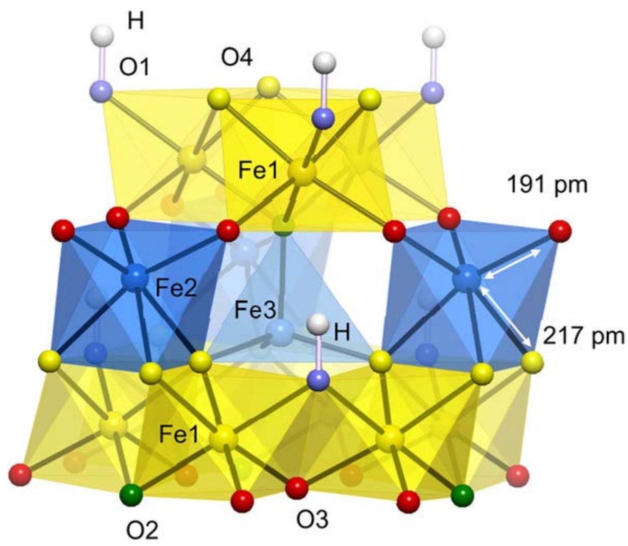

Figure 1.2. Keggin moiety of the ideal ferrihydrite structure (Heimestra 2013)

The reactivity of Fh vis-à-vis adsorption of ions and molecules can then be rationalized based on the new structural model and will hence depend mostly on the existence of singly coordinated surface functional hydroxyl groups. Two types of singly-coordinated surface groups interact with ions at the surface of Fh. The first type forms the edge of exposed Fe octahedra suitable for the formation of bidentate inner-sphere complexes, while the other type located at a single corner of two adjacent Fe octahedra provides appropriate sites for double-corner bidentate complexes [10].

1.3 Aluminum Substituted Fh

In natural environments, pure Fh is uncommon since it readily reacts with impurities that are often incorporated in the structure through co-precipitation, structural substitution, and surface adsorption, which leads to variable chemical compositions and surface properties. Aluminum (Al) is one of the most common substituents and co-precipitates with Fh [3, 17-19]. The incorporation of Al(III) in the Fh structure causes a critical impact on the structure, composition, and sorptive properties of Fh leading to substantial variability in surface reactivity of Fh [18-31]. Recently, the mechanism by which Al (III) is incorporated in the Fh structure has been studied and it is reported that up to 20-30 mol % of Al(III) can be substituted in Fh structure, while with more than 30 mol % of Al(III), a secondary Al(III) hydroxide phase, such as gibbsite, is formed by co-precipitation [21, 32-33].

1.4 Oxyanions

A chemical compound with the general formula $A_xO_Y^{z-}$ is called an oxyanion (or oxoanion) where A and O denote a chemical element and an oxygen atom, respectively [2, 34]. These compounds composed of non-metal elements in the group IIIA to VIA form in aqueous solutions. The pH and dissociation constants of any particular oxyanion determine their negative charge [35]. Some of the oxyanions commonly found in the natural environment are: borate (BO_3^{3-}), carbonate (CO_3^{2-}), nitrate (NO_3^{-}), phosphate (PO_4^{2-}), sulfate (SO_4^{2-}), chromate (CrO_4^{2-}), arsenate (AsO_4^{3-}), nitrite (NO^{2-}), arsenite (AsO_3^{3-}), etc [3, 36]. In this study, we have chosen to study chloride, nitrate, phosphate, sulfate, and arsenate (Appendix A.1). This choice was guided by their environmental relevance, their expected interaction strength, and their expected effect on the surface as these oxyanions have been reported to exhibit markedly different interactions with Fh surfaces. The observed surface complexes are outer-sphere complexes for chloride and nitrate [3, 36-37], a mixture of outer-sphere/inner-sphere for sulfate [19, 38-40] and inner-sphere for phosphate and arsenate [40-44]. Arsenic is a toxic element for animals, plants, and humans, and can be leached to the groundwater and contaminate both soils and water bodies. [45]. The mobility and bioavailability of geogenic and anthropogenic arsenic are controlled to a great extent by its sorption to natural minerals [46-47]. Arsenate with plus five oxidation state (+V) is one of two primary inorganic forms of arsenic that is dominant under oxic conditions. The other form of arsenic is arsenite with plus three oxidation state (+III). It is more soluble and toxic than arsenate [48-50].

Among all the oxyanions, phosphate has the most similar chemical properties to arsenate. Both of them are tetrahedral oxyanions from Group V elements and compete for adsorption sites on aluminum oxides, iron oxides, and 1:1 silicate clays (e.g., kaolinite) [51-53]. Despite their chemical similarity, the biological behaviors of phosphate and arsenate are significantly different since phosphate is not known as a natural or anthropogenic contaminant. Although the excessive phosphorus in aquatic environment may result in eutrophication, it is an essential nutrient for plant growth and is considered a macronutrient [42, 52]. Phosphate with three OH groups exhibits a complex speciations distribution of H_3PO_4, $H_2PO_4^-$, HPO_4^{2-}, and PO_4^{3-} depending on the solutions chemistry and pH [35, 54].

Sulfur is also an essential nutrient for plant growth. The dominant form of sulfur is sulfate which is also less toxic and problematic than arsenate. However, sulfate is a common acid-producing contaminant prevalent in acid-mine drainage and impacting the quality of soil and water resources [48]. In the aquatic environment, sulfate minerals such as $CaSO_4$(s) and $MgSO_4$(s) can be readily dissolved and release sulfate to surface or ground waters [3]. Similarly to arsenate and phosphate, sulfate competes with other oxyanions for the available sites on mineral surfaces. Adsorption of sulfate can impact many processes that happen at the water-mineral interface such as the dissolution of iron oxides, the activity of catalysts, and electrochemical properties of minerals [55]. The fate and transport of base cation nutrients such as Ca^{2+} and Mg^{2+} in forest soil are also controlled by sulfate adsorption where sulfate acts as an indirect conserver of these cations [54].

Nitrogen is the most critical macronutrient required by plants [56]. Nitrate, ammonium, and dinitrogen are the available inorganic forms of nitrogen in the soil [57]. However, nitrate is the primary source of nitrogen in many soils and is critical for plant growth [58]. The variation in nitrate concentration in the soil can even occur seasonally. The significant uptake of nitrate during the spring or massive seasonal rain events may give rise to depletion of nitrate in the soil and transport to surface and ground waters [56]. The excessive amount of highly soluble and stable nitrate in the aquatic environments lead to eutrophication of water bodies endangering marine life and humans and animals drinking those waters [57, 59].

Another anion studied in this project is chloride (Cl^-). It has similar chemical properties to those of nitrate as they are both monovalent and compete with each other for surface sites. Chloride and nitrate are considered exchangeable ions in mineral-water interface systems and can easily replace each other [3, 36, 60-61]. In soil systems, chloride is the only stable oxidation state and is not as critical as nitrate for plant growth but may also be considered as a micronutrient for higher plants [62].

1.5 Overview

The overall objective of this work is to examine the interaction, adsorption/desorption, and reversibility of five oxyanions on Fh using mostly the thermodynamic data acquired by flow microcalorimetry. In addition, the role of Al(III) incorporation on the physical and chemical properties of Fh is investigated.

In Chapter 2, the adsorption of phosphate, sulfate, arsenate, chloride, and nitrate on Fh is examined at pH 5.6 and the enthalpy of the interaction is calculated for each anion. In Chapter 3, the adsorption/desorption and reversibility of sulfate on three different Fhs with varied aluminum concentration are examined at both pH 5.6 and 3.0 to indirectly assess the role of Al(III) incorporation on the underlying SO_4 binding modes.

2 THE ENERGETICS OF OXYANION SORPTION ON FERRIHYDRITE STUDIED USING FLOW MICROCALORIMETRY

2.1 Introduction

Adsorption is one of the most important mechanisms by which nutrients, pollutants, and other solutes are distributed in natural environment between solid, aqueous, and gas phases [2-5, 36]. Adsorption occurs as a substance is accumulated at the interface between two phases particularly in the solid-liquid interface[2, 36, 63] and controls a wide variety of processes such as mineral weathering kinetics[64], nucleation and crystal growth[65], natural organic matter stabilization, and solute transport[66].

Oxyanions are common metals and metalloids of high ionic potential from the group IIIA to VIA of the formula A_XOy. They are formed in aqueous solutions in which their charged species are determined by the solution chemistry (pH, ionic strength, and composition) and their dissociation constants. Oxyanions possess a high affinity for sorption on surfaces of metal (hydr) oxides such as those of Al and Fe, particularly in acidic to intermediate pH values where these surfaces are dominated by a positive charge[2]. For example, ferrihydrite (Fh), a semicrystalline iron (hydr) oxide, provides enough positive surface charge for oxyanions adsorption in soil and groundwater to promote either electrostatic adsorption or ligand exchange through complex formation[2, 6-8, 40].

The oxyanions chosen for this work are chloride, nitrate, sulfate, phosphate, and arsenate, a choice guided by their environmental relevance and their placement along the well-known Hofmeister series. The mechanisms and binding mode of the adsorption of these oxyanions on iron (hydr) oxide surfaces in general, and Fh in particular have been extensively investigated [42 44, 53, 55, [67-73]. On Fh, an electrostatic (outer-sphere) adsorption is usually reported for chloride and nitrate[3, 36-37, 74], and inner-sphere complexation dominated by bidentate surface complexes for phosphate and arsenate[42-44, 50]. Sulfate has been found to form both outer-sphere and inner-sphere complexes[19, 38-39].

Despite the extensive research investigating the surface complexation of these oxyanions on aluminum and iron oxide surfaces, very few studies have sought to determine the energetics and thermodynamics of their interactions, particularly studies that have directly measured these values in a systematic and consistent way. When available, these data have been inconsistent. For instance, using the temperature dependence of sorption isotherms, phosphate adsorption was reported to be endothermic in some studies[75-76] and exothermic in others [77-78]. There are limited studies using calorimetry to directly measure the energetics and enthalpies of adsorption (ΔH_{ads}) for some of these oxyanions. For instance, Kabengi et al. [69] recently published a study combining flow adsorption microcalorimetry (FAMC) with attenuated total reflection infrared (ATR FTIR) spectroscopy and density functional theory (DFT) calculations to study chromate complexation on hematite (Hm) and ferrihydrite (Fh). The authors reported that chromate binds exothermically in an inner-sphere mode on both solids, with a ΔH_{ads} of −6.3 kJ/mol and −7.38 kJ/mol, for Hm and Fh respectively. Similarly, other studies also using flow microcalorimetry have published molar enthalpies of adsorption for several other oxyanions on a range of minerals, e.g., amorphous aluminum hydroxide[37, 61, 79], boehmite[80], mixed Al (III)–Fe (III) hydr (oxide)[74], and hematite[81-82]. The ΔH_{ads} values for oxyanions adsorption on amorphous aluminum hydroxide were found to be +2.9 ± 1.4 kJ/mol for sulfate and −6.5 ± 3 kJ/mol for phosphate[79], and ranging from −3.0 to − 66 kJ/mol for arsenate[61].

These inconsistencies in the thermodynamics values and the piecemeal nature of the very few ΔH_{ads} measured underscore the need to conduct a systematic study of the adsorption of oxyanions on one surface to allow for a direct comparison absent of variability factors from either the solid or aqueous phase. To that end, this work will use flow microcalorimetry (FMC), to directly measure the energetics and enthalpies of adsorption of chloride, nitrate, sulfate, phosphate, and arsenate on freshly synthesized 2-line Fh samples. These anions are expected to exhibit a suite of complexation mechanisms varying from electrostatic outer-sphere surface complexes on one end to inner-sphere complexation on the other. Our hypothesis is that the strength of their interactions will be reflected in the values measured and by their effect on the positive surface charge. To our understanding, this is the first experimental study that encompasses this range of oxyanions adsorbed on the same solid.

2.2 Materials and Methods

2.2.1 Chemicals

The oxyanions used in this study include chloride (NaCl, 99.0 %+), nitrate ($NaNO_3$, 99.8 %), sulfate (Na_2SO_4. 99.7%), phosphate ($Na_2H_2PO_4$. H_2O, 99.6%), and arsenate (Na_2HAsO_4. $7H_2O$, 98.0%). All salts, acids, and bases used were ACS reagent grade chemicals and used as received except for the two anhydrous salts ($NaNO_3$ and NaCl) that were kept in a dry oven at 65 °C. Solutions were freshly prepared in 18.2 MΩ water and adjusted to pH 5.6 ± 0.1 using dropwise additions of 0.1 M HNO_3 or 0.1 M NaOH that had a negligible impact on the ionic strength of the solutions.

All solutions were made in a background of NaCl keeping the total concentration of Na^+ at 0.05 M and the ionic strength constant. The concentrations of the oxyanion and NaCl for each solution are presented in Table.2.1

Table 2.1. Experimental conditions for the adsorption experiments.

Experiment Name	NaCl M	$NaNO_3$ M	Na_2SO_4. M	$Na_2H_2PO_4 . H_2O$ M	$Na_2HAsO_4 . 7H_2O$ M
Chloride	5×10^{-2}	0	0	0	0
Nitrate	0	5×10^{-2}	0	0	0
Sulfate	35×10^{-2}	0	5×10^{-3}	0	0
Phosphate	5×10^{-2}	0	0	5×10^{-4}	0
Arsenate	5×10^{-2}	0	0	0	5×10^{-4}

These values were chosen based on results from preliminary tests and prior work to ensure that the adsorption reaction would come to completion in a reasonable time frame and that an accurate mass balance would be possible.

The chemistries of sulfate, phosphate, and arsenate solutions outlined in Table 2.1 were modeled using Visual Minteq. Visual Minteq indicated that the solution containing sulfate should have SO_4^{2-} as the dominant sulfate species (90 %), the solution containing phosphate should have $H_2PO_4^-$ as the dominant species (89 %), whereas $H_2AsO_4^-$ was the dominant species (93 %) in the solution containing arsenate (Table 2.2).

2.2.2 Characterization

The Schwertmann and Cornell's protocol was used to synthesize 2-line Fh [83]. Accordingly, a solution of 0.2 M Fe $(NO_3)_3$ (ACS grade, Fisher Scientific) was titrated to pH 7.5 through the addition of a 150 mL of a 1 M KOH solution. The resulting suspension was centrifuged and dialyzed against ultra-pure water (18.2 MΩ) for several days until the conductivity of the water

Table 2.2. The speciation of the oxyanions under the experimental conditions.

Experiment Name	Species formula	% of total concentration
Sulfate	SO_4^{-2}	90 %
	$NaSO_4^{-}$	10 %
Phosphate	$H_2PO_4^{-}$	89 %
	HPO_4^{2-}	4 %
	NaH_2PO_4 (aq)	6%
Arsenate	$H_2AsO_4^{-}$	93 %
	$HAsO_4^{-2}$	7 %

dropped below 20 µS.cm^{-1}. The suspension was then air-dried under the hood for 24 hours and ground into fine powders using an agate mortar and pestle. The Fh used in each experiment was freshly synthesized and utilized within 1-2 days.

Fh synthesis and X-ray diffraction (XRD) patterns were obtained from a Panalytical XPert Pro MPD instrument using CuKα radiation at generator settings operating at 45 kV and 40 mA which indicated the sample was amorphous (Appendix B.1). Samples were out-gassed for 12 h at 50 ºC to remove any adsorbed volatile compounds from the surface and BET surface analysis (Quantachrome AS1Win, Quantachrome Instruments) was conducted using N_2 gas. The specific surface area was determined to be 368 m^2/g. The morphology and size of the Fh nanoparticles were characterized by high resolution transmission electron microscopy (HRTEM; JEOL 2100F operating at 200 kV) and revealed no well-defined crystal faces and a particle size of roughly 3 nm (see TEM images in Appendix B.2).

2.2.3 Experiments

The flow microcalorimeters (FMC) used to conduct the experiments were custom-designed and fabricated in the Kabengi laboratory at Georgia State University. The description of the instrument and basic experimental procedures have been discussed in previous publications [37, 61, 84] and are included in Appendix B.4.

A known mass of Fh sample (~ 45.5 mg for sulfate and ~ 5.0 mg for all other oxyanions) was packed in the sample holder of the instrument's column and flushed with 0.05 M NaCl until a steady baseline representing thermal equilibrium was reached. The input solution was then switched to 0.05 M $NaNO_3$, and the calorimetric signal associated with NO_3^- exchanging with Cl^- ([C/N]) on the surface was recorded. After the calorimetric signal returned to the original baseline, the solution was switched back to 0.05 M NaCl and the calorimetric signal of Cl^- replacing NO_3^- ([N/C]) obtained. This cycle was repeated over 2 days until the heat of exchange (Q_{exch}) for 3–5 replicates of each exchange leg ([C/N] and [N/C]) was constant indicating the surface was equilibrated and ready for further experiments.

Both Cl^- and NO_3^- have been reported to undergo a reversible outer-sphere ion exchange reaction on Fh [3, 36-37, 61, 69, 74] and are therefore excellent *in situ* calorimetric probes of the surface positive charge. Thus, in addition to measuring the energetics of their interactions with the Fh sample, the exchange cycles of Cl^- and NO_3^- were used to measure the reversibility of the interaction of the other oxyanions (sulfate, arsenate, and phosphate) as described below.

For each experiment, once the Q_{exch} of C/N and N/C cycles had stabilized, a stable baseline was obtained in 0.05 M NaCl. The input solution was then switched to 0.035 M NaCl + 0.005 M Na_2SO_4, 0.05 M NaCl + 0.0005 M $Na_2H_2PO_4$, and 0.05 M NaCl + 0.0005 M Na_2HAsO_4 for sulfate, phosphate, and arsenate experiments respectively to obtain the calorimetric response of their interactions with the Fh. After the completion of these reactions as indicated by a return to the initial baseline, the solution was reverted back to 0.05 M NaCl, and additional [C/N] and [N/C] cycles were conducted as described above until no further change in the magnitude of 5 consecutive cycles was detected. Throughout the Fh exposure and subsequent C/N and N/C cycles, effluent samples were collected and the total aqueous concentration of oxyanions determined using High-Performance Liquid Chromatography – Ion Conductivity (Metrohm, 881 compact IC pro). The mass of oxyanions retained and subsequently desorbed from the surface was determined by a mass balance calculation between the mass injected, and that recovered in all effluents.

2.3 Results and Discussion

2.3.1 Energetics of Exchange and Adsorption

The calorimetric signals and Q for all the oxyanions exchanging with chloride were exothermic while the heat of exchange (Q_{exch}) of [N/C] was endothermic (Figure 2.1). Additionally, the reactions of these anions with the Fh surface took different times to reach thermal equilibrium. For [C/N] and [N/C] the reaction time was 30 min, for sulfate ([C/S]) it took around 40 min, as for phosphate ([C/P]) and arsenate ([C/As]) the return to baseline was significantly slower and took 50 min.

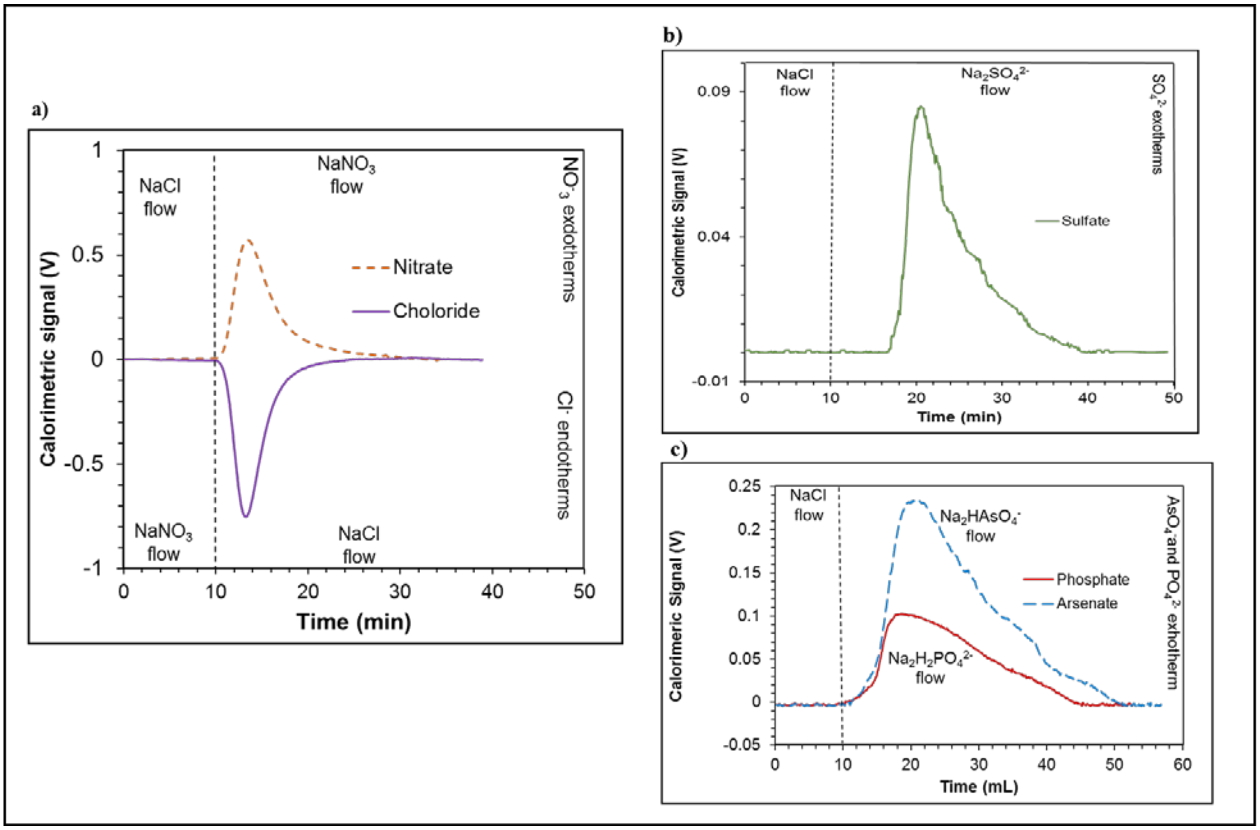

Figure 2-1. The calorimetric signal for a) chloride and nitrate exchange, b) sulfate adsorption and c) phosphate and arsenate adsorption. An increase in voltage resulting in a positive peak corresponds to a release of energy and hence an exothermic reaction. Conversely, a decrease in voltage resulting in a negative peak corresponds to energy consumption and hence an endothermic reaction. The concentrations of each oxyanion in solutions are 0.05 M chloride and nitrate, 0.005 M for sulfate and 0.0005 M for phosphate and arsenate. The mass of solid used for sulfate is ~ 45 mg, and between 3 to 5 mg for the other oxyanions.

The heats of exchange (Q_{exch}) for all reactions are summarized in Table 2.3. Q_{exch} for [C/N] and [N/C] were similar in magnitude at - 2.26 ± 0.16 for [C/N] and 2.18 ±0.11 for [N/C]. The correspondence of their Q_{exch} and their reactions times and peak areas further confirm that the exchange of Cl^- and NO_3^- is indeed reproducible and reversible as previously reported [37, 79, 84]. On the other hand, as hypothesized $Q_{exch/ads}$ for the other oxyanions did reflect the strength of their interactions with Q_{ads} measured at -12.74 mJ/mg for arsenate, -5.440 mJ/mg for phosphate and -0.170 mJ/mg for sulfate.

Table 2.3. Summary of the heat of exchange values corresponding to the adsorption of oxyanions.

Anions	**pH**	**Concentration (mM)**	**Amount adsorbed (umol/mg)**	**amount adsorbed (μmol/m²)**	**Q_{ads} (J/mg)**	**Enthalpy (kJ/mol)**
Arsenate	5.6(0.02)[1]	0.5	0.56	1.51[2]	-12.74	-22.86
Phosphate	5.6(0.02)	0.5	0.90	2.46	-5.440	-6.01
Sulfate	5.6(0.02)	5	0.56	1.52	-0.17	-0.30
Nitrate	5.6(0.02)	50	65.27	177.37	-2.26 (0.16)	-0.03
Chloride	5.6(0.02)	50	169.78	461.35	2.18 (0.11)	0.01

[1]*Numbers in parenthesis correspond to the standard error*
[2]*The specific surface area used to calculate the surface excess ($\mu mol/m^2$) is 368 m^2/ g*

The mass adsorbed and surface excess of each oxyanion are presented in Table 2.3 and demonstrate that in each case a different adsorbed mass is required to reach surface saturation. Although at different initial solution concentrations, for both sulfate (0.005 M) and arsenate (0.0005 M), 0.560 µmol/mg of the injected mass was adsorbed. The adsorbed mass was higher for phosphate (0.0005 M) as 0.900 µmol PO_4^{2-}/mg of the mass injected was retained at the surface. Whereas for chloride (50 mM) and nitrate (50 mM), there was significantly more adsorbed as we measured 62.27 µmol NO_3^-/mg and 169.78 µmol Cl^-/mg for chloride. The ΔH values (kJ/mol) at maximum coverage were -22.86 kJ/mol for arsenate, -6.01 kJ/mol for phosphate, -0.30 kJ/mol for sulfate, 0.03 kJ/mol for nitrate, and 0.01 kJ/mol for chloride adsorption on the surface, and hence increased following a positive Hofmeister series such that $\Delta H_{Cl^-} = \Delta H_{NO_3^-} < \Delta H_{SO_4^{2-}} < \Delta H_{PO_4^-} < \Delta H_{AsO_4^{2-}}$. As already stated, the energetics and enthalpies of the adsorption of these oxyanions on Fh have not been largely studied. However, there are some works that have studied these mechanisms on some other solids. For example, Appel et al. [79] reported the molar heats of sorption of sulfate and phosphate on aluminum hydroxide at +2.9 ± 1.4 kJ/mol and −6.5 ± 3 kJ/mol, respectively. Also, Kabengi et al. [61] measured the molar heats of arsenate sorption on the aluminum hydroxide which was from −3.0 to −66 kJ/mol. Machesky et al. [85] also measured the enthalpy of adsorption of phosphate on goethite which was from -15 to – 25 KJ/mol in different surface coverage.

Although it is necessary to conduct more experiments to ensure the numbers obtained are significantly representative of a larger set of Fh samples, these values qualitatively provide insights into the adsorption mechanisms of different anions on the Fh surface. Both phosphate and arsenate have been reported to complex strongly via inner-sphere complexes [40, 42-44] and their ΔH_{ads} values, which are in good agreement with our results, are the most exothermic among all the oxyanions studies. Antelo et al. [42] showed that the adsorption of phosphate on Fh at pH values between 5 to 6 is slightly higher than that of arsenate, which is also consistent with our findings. However, the reason for the higher value of ΔH for arsenate than phosphate is not well known. This discrepancy may be attributed to the difference between the ratio of monodentate and bidentate complexes formed by arsenate and phosphate. Arsenate is mostly bound to Fh as bidentate corner sharing complexes, and the formation of the monodentate complex is not significant (~ 15%) and even decreases with increasing pH [42, 86]. However, a mixture of monodentate and bidentate binuclear species have been reported for complexation of phosphate on iron hydroxides in acidic to intermediate pHs [40, 87-88]. Arai and Sparks [43] suggested bidentate binuclear complexes co-existing with monodentate mononuclear species at pH >7.5 for phosphate. On the other end of the spectrum, chloride and nitrate complex through outer-sphere electrostatic mechanisms and they do indeed possess a very small, almost negligible enthalpy as expected.

Conversely to other oxyanions, a mixture of inner-sphere and outer-sphere species has been suggested for sulfate complexation [19, 38-40, 73]. The contribution of outer-sphere species to sulfate complexion may justify the low ΔH measured compared to phosphate and arsenate. Gu et al. [39]

proposed that for air-dried Fh samples, with increasing pH and decreasing ionic strength, the outer-sphere species increases such that for pH values between 5 to 6 and ionic strength (I) of 0.02 M, more than 70% of sulfate is bound as outer-sphere species through electrostatic interactions and a smaller fraction exists as bidentate-binuclear inner-sphere complexes. As such, at the pH 5.6 and the ionic strength 0.05 M used in this work, the predominant mode of complexation for the sulfate adsorption was likely outer-sphere complexes which is consistent with the very low molar enthalpy measured for sulfate adsorption.

2.3.2 Desorption and Reversibility

As stated, the reactions of both chloride and nitrate with Fh surface are reversible, and as such, they are excellent probes of the surface positive charge and the effect of the other oxyanions adsorption on it. This is achieved by comparing the magnitudes of Q_{exch} before and after exposing the surface to the other oxyanions. Furthermore, the changes in Q_{exch} with time, if any, as the surface is exposed to increasing volumes of solution through additional exchange cycles, are good indicators of the adsorption reversibility. The magnitude of the calorimetric signals for [C/N] cycles of all the experiments decreased since the oxyanions occupy the same charge-bearing functional groups which are no longer available for ion exchange (Table 2.4). The reduction in the first post-treatment Q_{exch} of [C/N] was not similar for all oxyanions studied. Compared to the pre-treatment Q_{exch}, the observed reduction was by 74.3 % for arsenate, by 60.6 % after phosphate and 42.3 % post sulfate. However, with subsequent [C/N] and [N/C] exchange cycles, the Q_{exch} values gradually increased back. We considered the point in time where no further change in the Q_{exch} of 5 consecutive peaks was observed to represent post-treatment equilibrium. Furthermore, the volumes required to reach post-treatment equilibrium were different. The posttreatment equilibrium Q_{exch} of [C/N] occurred at a fraction of their pre-adsorption values. These were at 99%

Table 2.4. The heat of exchange for the representative pretreatment [C/N], the first posttreatment [C/N] and the equilibrium posttreatment.

Anions	Q_{exch} for the pretreatment [C/N] (mJ/mg)	Q_{exch} for the first posttreatment [C/N] (mJ/mg)	Reduction in Q_{exch} for the first posttreatment [C/N] %	Q_{exch} of equilibrium posttreatment [C/N] (mJ/mg)	Q_{exch} of equilibrium posttreatment [C/N] %
Arsenate	-2.430 (0.267)[1,2]	-0.65	73.3	-1.080 (0.108)	44.4
Phosphate	-2.934 (0.176)	-1.156	60.6	-1.488 (0.210)	50.7
Sulfate	-1.980 (0.06)	-1.143	42.3	-1.960 (0.100)	99.0

[1]Numbers in parenthesis corresponds to the standard error
[2]Heats of exchange in this table are listed as negative numbers as the heat of exchange of nitrate replacing chloride was used as it is the first exchange after adsorption which can be compared with the pretreatment values.

for sulfate, 50.7% for phosphate and 44.4% for arsenate.

The desorption of phosphate, arsenate, and sulfate by chloride and nitrate was slower compared to their adsorption and was incomplete even after 40-50 times more volume of NaCl, and $NaNO_3$ solutions was passed through the cell compared to the volume required to reach surface saturation during the adsorption process. For sulfate experiments, it took ~ 750 mL of cumulative volume to recover 99 % of the Q_{exch} after sulfate, 54 mL to recover 50.7 % of Q_{exch} after phosphate and 170 mL to recover 44.4% after arsenate.

The reversibility data is in a good agreement with the results from the energetics of exchange and adsorption as with increasing ΔH_{ads} values, the reduction in the first posttreatment Q_{exch} of [C/N] and irreversibility increases. In general, the energetics and the impact on the surface charge strongly mirrored the previously reported strength and mode of binding of the oxyanions with the Fh surface functional groups. The electrostatic interactions showed a constant and reversible Q_{exch} over repeated measurements, while the Q_{exch} values for anions interacting through ligand complexation exhibited a higher and more modulated reversibility behavior in that a higher fraction of arsenate adsorption was irreversible as it binds in inner-sphere bidentate binuclear complexes. The fraction of irreversible complexes decreases for phosphate as the fraction of monodentate mononuclear increases, and for sulfate which forms a significant fraction of outer-sphere complexes. On the other end, chloride and nitrate bind only as outer-sphere complexes and their reactions are entirely reversible.

2.4 Conclusion

Flow microcalorimetry was utilized in this work to obtain thermodynamic data for oxyanion adsorption on the Fh surface. The calorimetric signals for all of the oxyanions exchange and adsorption were exothermic, while an endothermic heat of exchange was detected for chloride replacing nitrate. The reactions of both the [C/N[and [N/C] with Fh surface were reversible, while other oxyanions showed irreversible reaction such that 99 % of the sulfate, 50.7% of phosphate and 44.4 % arsenate were desorbed from the surface after subsequent C/N and N/C cycles. The molar enthalpy of the oxyanions adsorption on Fh increased following a positive Hofmeister series and mirrored the strength and mode of surface complexation (i.e., $Cl^-<NO_3^-<SO_4^{2-}< H_2PO_4^-< H_2AsO_4^-$) from electrostatic outer-sphere in $Cl^-<NO_3^-$, a mixture of outer-sphere and inner-sphere complexations in $<SO_4^{2-}$, monodentate-bidentate inner-sphere in $<H_2PO_4^-$ to bidentate inner-sphere in $H_2AsO_4^-$. Also, the reduction in first posttreatment heat of exchange and irreversibility followed the same trend, increasing with increasing molar enthalpy across the oxyanions. Overall, based on the results obtained in this work, it can be concluded that the energetic and reversibility of oxyanions adsorption on Fh is correlated with the different type of surface complexations.

3 THE ROLE OF ALUMINUM SUBSTITUTION INTO FERRIHYDRITE ON THE MECHANISMS OF THE SULFATE ADSORPTION/DESORPTION.

3.1 Introduction

Ferrihydrite (Fh) is one of the most reactive nanocrystalline iron (hydr) oxides in abiotic and biotic environments [89-92]. Because of its high specific surface area and high density of reactive surface-sites, Fh plays a critical role in determining the fate and transport of nutrients and contaminants [19, 39, 92-93]. Recently, Michel et al. [9] proposed a new model for the structure of Fh revealing that in addition to having Fe in hexacoordination, Fh contains Fe in tetrahedral coordination (~ 20%) as well. Based on this model, Hiemstra [11] developed a quantitative surface depletion (SD) model to elucidate the surface structure and composition of Fh evaluating type and number of reactive surface sites, corresponding proton affinities and point of zero charge (PZC).

In aquatic and terrestrial environments, Fh readily reacts with impurities, such as aluminum (Al), to form variably substituted chemical compositions. The substitution of Al (III) in the Fh structure impacts its structure, composition, and sorptive properties causing substantial variability in terms of reduction potential [7, 27, 94], Fe (III) bioavailability [27, 29, 95], secondary mineralization to hematite and goethite [26, 29, 96], desorption of aqueous contaminants [25, 97-98], solubility [28, 53, 99] as well as sorption reactions [19, 21, 25]. Cismasu et al. [100] sampled and characterized naturally-occurring ferrihydrites from an acid mine drainage site to study the impact of impurities such as Aluminum (Al^{3+}), Silicon (Si^{4+}), and organic matter on Fh structures. These researchers found that 1) Si^{4+} is complexed at the surface of Fh and affects its crystallinity, 2) Al^{3+} substitution does occur for Fe^{3+}, and 3) association of organic matter with Fh aggregates contributes to more structural disorder in ferrihydrite. Adra et al. [97] showed that in an area affected by an arsenic-rich acid mine drainage, Fh has a particular role in removing the arsenic from a river bed sediments with approximately neutral pH. Characterizing the natural Fh associated with Al (III), and comparing it with the synthetic Al-substituted samples indicated inner-sphere surface complexes of As (V) on both the natural and synthetic Al-substituted Fh. Cismasu and co-workers [18, 21, 101] studied properties of impurity-bearing Fh by synthesizing Al-bearing Fh samples containing from 5% mol Al (III) to 40% mol Al precipitated in two modes: a slow and a fast titration. They then used a suite of laboratory and synchrotron-based techniques (X-ray Pair Distribution Function analysis (d-PDF) analysis, scanning transmission X-ray microscopy (STXM), Al K-edge X-ray absorption near edge structure Al K-edge XANES spectroscopy) to characterize the structural properties of the solids obtained. Although a small amount of separate aluminous phases (<6%) was detected by NMR for 15 mol% Al (III) samples, they concluded that regardless of the titration speed octahedrally-coordinated Al (III) is substituted in the Fh structure in samples with a concentration up to 20-30 mol%, while at higher Al content gibbsite, a secondary Al (III) hydroxide phase, is formed by co-precipitation. Similarly, Manceau and Gates [33] proposed that in agreement with Pauling's distortion rule, Al-Al avoidance governs the saturation limit of Al (III) substitution in the Fh structure, and predicted this substitution to occur up to 25 molar % for Fh and 30 molar % for goethite. The impact of Al (III) substitution in Fh on the surface interactions with primary cationic and anionic contaminants have also been investigated, albeit to a lesser extent. There have been several studies investigating the adsorption of oxyanions on Fe (III) oxyhydroxy minerals[19, 38-39, 74, 102-106]. Among all oxyanions sulfate, for example, is of particular interest as it is a common anion in water, soil and atmospheric environments. Sulfate is the byproduct of acid-forming processes in soils and impacts the bioavailability of sulfur to plants, adsorption of other organic and inorganic contaminants, and element cycling [39-40, 67, 71, 107-119].

Generally, a mixture of inner-sphere and outer-sphere species has been reported for the complexation of sulfate on Fh [19, 38-40, 73]. Zhu et al. [120] used infrared spectroscopic analysis, sulfur K-edge extended X-ray absorption fine structure (EXAFS) spectroscopy, and d-PDF analysis to study the structure of sulfate adsorption complexes on air-dried Fh samples. They reported both inner-sphere bidentate −binuclear and outer-sphere species were adsorbed. Gu et al. [39] combined sulfur K-edge XANES and EXAFS spectroscopy, quantum chemical calculations, and surface complexation modeling (SCM) and found that the relative fractions of inner-sphere and outer-sphere complexes depend on the pH, ionic strength (*I*), and whether the sample is either air dried or kept wet. Some of their specific conclusions are that the relative fraction of inner-sphere complexes is constant at different ion strengths, whereas it decreases with increasing pH. In contrast, outer-sphere complexes vary with both *I* and pH. The authors also demonstrate that the inner-sphere complexation is more favored in samples that have been air dried, whereas, in the presence of hydration, more outer-sphere complexes are formed. Thus, the dehydration state of the sample affects the ratio of outer-sphere to inner-sphere complexes. Johnston and Chrysochoou [19] used in situ ATR-FTIR spectroscopy to study the adsorption mechanism of sulfate and two other oxyanions, selenate, and chromate, on Al-ferrihydrites, and reported that regardless of pH, the increase in the Al (III) concentration significantly enhances outer-sphere complexation for all the oxyanions studied.

The goal of this work is to use sulfate as a probe to study the impact of Al (III) substitution in Fh on its sorptive capacity. Sulfate has been chosen since it allows us to investigate both inner-sphere and outer-sphere complexation. Flow microcalorimetry (FMC) will be employed to systematically measure the energetics of sulfate adsorption/desorption, as well as its impact on the surface charge to further understand the mechanisms by which Al (III), and potentially other impurities, affects the specific modes of complexation of potential contaminants in natural environments. To our knowledge, there is only one published paper studying the adsorption of sulfate on AlFh [19] and, as far as thermodynamic data is concerned, only one other paper investigated the energetics of sulfate adsorption on amorphous aluminum hydroxide [79].

3.2 Materials and Methods

3.2.1 Mineral Synthesis

Al-substituted ferrihydrites were prepared according to a modified Schwertmann and Cornell's protocol [83] for the synthesis of 2-line Fh. Specifically, 0.2M $Fe(NO_3)_3$ and 0.2M $Al(NO_3)_3$ (ACS grade, Fisher Scientific) solutions were prepared and mixed to obtain 200 mL solutions at Al molar percentages of 0, 12 and 24. While continuously monitoring the pH, these mixed Fe and Al solutions were titrated to pH 7.5 with the addition of a 1 M KOH solution that was prepared the same day. This titration resulted in the total addition of 150 mL KOH in approximately 25 minutes and is considered a slow titration (Cismasu et al., 2013). The resulting suspensions were centrifuged and dialyzed against ultra-pure water (18.2 MΩ) for several days until the conductivity of the solutions dropped below 20 $\mu S\ cm^{-1}$. The suspensions were air-dried for 24 hours and ground into fine powders using an agate mortar and pestle to yield three samples: 0AlFh (pure ferrihydrite), 12AlFh (12 mol % Al) and 24AlFh (24 mol %). For each experiment, samples were freshly prepared and used within 2 days.

3.2.2 Sample Characterization

The chemical elemental composition of the samples was determined by Inductively Coupled Plasma- Atomic Emission Spectroscopy (ICP-AES) using an ARL 3560 ICP analyzer.

The samples were digested using the standard EPA 3050 method [121]. X-ray diffraction (XRD) patterns were obtained on a Panalytical XPert Pro MPD instrument operating at 45 kV and 40 mA using CuKα radiation, a 1/4° programmable divergence slit and a graphite monochromator on the diffracted beam at generator settings operating at 45 kV and 40 mA. To obtain specific surface areas (SSAs) of air-dried samples, multipoint Brunauer-Emmet-Teller (BET) N_2 adsorption isotherms were conducted using a Quantochrome NovaWin surface area analyzer. The general morphology of the samples was studied by high resolution transmission electron microscopy (HRTEM) using a JEOL 2100F instrument operating at 200 kV (JEOL, Ltd. Tokyo Japan). Samples were deposited on a copper specimen grid coated with an ultrathin layer of carbon (Ted Pella, Inc.) and kept in a hood to evaporate excess methanol. Energy dispersive X-ray spectroscopy (EDS; Oxford detector) was used to obtain information on the elemental composition of the samples, while their crystallinity and mineral identity were verified by capturing electron diffraction patterns from selected areas of the samples.

Zeta potential measurements (Malvern Nano) were conducted on all three samples as a function of pH. Suspensions (0.5 g/L) were prepared in 0.05 M $NaNO_3$ and their pH adjusted with aliquots of 0.1 M NaOH to achieve pHs from 6.5 to 11. After a 24 h equilibration on a shaker, the zeta potential and the suspension pH were determined in triplicate.

3.2.3 Calorimetric Measurements

The flow microcalorimeters (FMC) used in this study are custom-designed and were built in the Kabengi laboratory at Georgia State University. The instrumentations' description and operational procedures have been previously published [37, 61, 84] and are included in section A.4 of the of the Appendix.

The impact of Al substitution on the mechanism of sulfate sorption was evaluated by measuring 1) the energetics of the interaction with the three AlFh samples at two pHs, (3.0 ± 0.1 and 5.6 ± 0.1, and 2) the change, if any, in the positive surface charge resulting from sulfate complexation as it occurs on the same charge-bearing surface hydroxyl functional groups. This change was measured using two anions, chloride (Cl^-) and nitrate (NO_3^-), that have been previously reported to undergo reversible outer-sphere ion exchange reaction on different Al- and Fe-oxides [37, 61, 74], and as such are excellent probes of the positive surface charge (Sabur et al., 2015; Kabengi et al., 2017). These anion exchange cycles were obtained as follows.

A known mass of AlFh sample (~ 5.0 mg for experiments at pH 3.0 and ~ 45.0 mg for those conducted at pH 5.6) was packed in the sample holder and flushed with 0.05 M NaCl until thermal equilibrium was achieved as indicated by a steady baseline. The input solution was then switched to 0.05 M $NaNO_3$, and the calorimetric signal corresponding to the displacement of Cl^- by NO_3^- ([C/N]) on the surface recorded. At the completion of the exchange, the solution was switched back to 0.05 M NaCl and the calorimetric signal of Cl^- exchanging with NO_3^- ([N/C]) obtained. These two solutions were cycled through until the surface was equilibrated and the heat of exchange (Q_{exch}) became constant for 3–5 replicates of each exchange cycle ([C/N] and [N/C]), which typically took 2-4 days. Because these exchange cycles are inherently time-based measurements, they were also used to assess the reversibility of the sulfate surface complexes. To that end, after exposing the samples to sulfate, additional [C/N] and [N/C] cycles were obtained until no further change in the magnitude of 5 consecutive cycles was detected.

Samples were exposed to sulfate by switching the input solution from 0.05 M NaCl to 0.035 M NaCl + 0.005 M Na_2SO_4. i.e. one in which 5×10^{-4} M NaCl has been replaced with 5×10^{-4} M sulfate while keeping the total concentration of Na at 0.05 M and the ionic strength (I) constant. After the thermal signature of the sulfate reaction has ended, which took between 60 - 140 min depending on the sample composition and pH, the input solution was reverted to 0.05 M NaCl. During the sulfate treatment and all subsequent chloride and nitrate exchange cycles, effluent samples were collected at a rate of 1 sample/5 min for chemical analysis. The total aqueous concentration of sulfate was determined using High-Performance Liquid Chromatography - ion conductivity (Metrohm, 881 compact IC pro). The chemistries of the 0.005 M Na_2SO_4 + 0.035 M NaCl M solution was modeled using Visual Minteq and indicated that the solution containing sulfate should have SO_4^{2-} as the dominant sulfate species (90 %).

The mass of sulfate retained at and subsequently desorbed from the surface was determined by a mass balance calculation between the mass of sulfate injected and that recovered in all effluents.

All salts used in microcalorimetry experiments were ACS certified and were used as received. All solutions were prepared using ultra-pure water (18.2 MΩ), were weakly buffered, and in equilibrium with pCO_2 in the atmosphere. The solution pH values were adjusted daily using dropwise additions of 0.1 M NaOH, 0.1 M HCl, 0.1 M HNO_3 for pH 5.6 ± 0.1 and 1 M HCl, and 1M HNO_3 for pH 3.0 ±0.1 experiments. These adjustments had a negligible impact on the concentration of the solutions.

3.3 Results

3.3.1 Characterization

A summary of the physical and chemical properties of the samples is shown in Table 1. Bulk XRD patterns (Appendix C.1) indicated that all samples were amorphous and that despite the increasing Al (III) content, there was no crystalline Al-(hydro) oxide phase, e.g., gibbsite. This finding is in line with previous studies where no gibbsite was detected below an Al (III) content of 30% [18-19]. A qualitative analysis of transmission electron micrographs revealed that increasing Al (III) content caused no significant variation in the general morphology and particle size that was roughly estimated at 3 nm in all three samples (Appendix C.3). EDS results obtained from multiple spots and particles from each sample presented consistent elemental profiles suggesting the Al (III) to be distributed homogeneously across the particles (Appendix C.3). The BET SSAs were 368 ± 14 m^2/g, 358 ± 28 m^2/g, and 363 ± 34 m^2/g for the 0AlFh, 12AlFh, and 24AlFh samples respectively. The isoelectric points (IEP) occurred at pH 8.0, 8.5 and 9.0 for the 0AlFh, 12AlFh, and 24 AlFh samples respectively (Appendix C.2). These values are in good agreement with the literature values obtained for Fh [11, 21], and for aluminum-bearing ferrihydrites [21, 99].

3.3.2 Chloride and Nitrate Exchange: Pre-Sulfate Treatment

Consistent with prior work [69, 82, 122], [C/N] exchange was exothermic and [N/C] exchange endothermic (Figure 3.1). The thermal responses associated with [C/N] and [N/C] cycles were similar in terms of reactions times, peak areas, and enthalpic sign confirming that the exchange of these two anions is indeed reproducible and reversible. It is noteworthy to remember that experiments at pH 3.0 were conducted with ~ 5 -6 mg of sample compared to ~ 40 - 45 mg for experiments at pH 5.6, and as such the raw calorimetric peaks shown in some of the figures can

Table 3.1. A summary of the physical and chemical properties of the samples

Sample (wt. %)	pH	Fe/(Al + Fe)/ mol %	Al/(Al + Fe)/ mol %	Surface Area m^2/g	Density (g/L)
0AlFh	5.6 (0.02)[1]	99.97 (0.3)	0.03 (0.00)	368.0 (14)	28.83 (2.09)[2]
12AlFh	5.6 (0.02)	89.14 (0.01)	10.86 (0.01)	358.0 (20)	26.01 (1.63)
24AlFh	5.6 (0.02)	77.91(0.09)	22.09 (0.02)	363.0 (24)	25.10 (1.63)
0AlFh	3 (0.03)	99.96 (0.3)	0.04 (0.00)	368.0 (14)	28.83 (2.09)
12AlFh	3 (0.03)	89.09 (0.3)	10.91 (0.01)	358.0 (20)	26.01 (1.63)
24AlFh	3 (0.07)	77.89 (0.06)	22.11 (0.01)	363.0 (24)	25.10 (1.63)

[1] *Numbers in parenthesis correspond to the standard error*

[2] *The density measured for the suspension of the fresh synthesized samples before air-drying decreased with increasing Al*

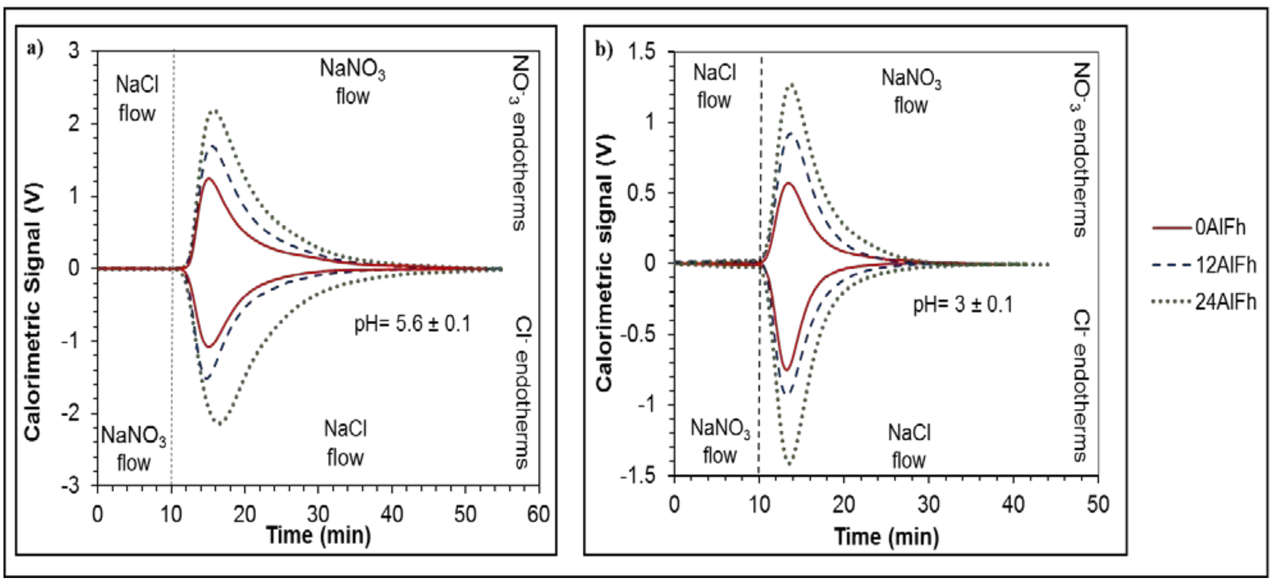

Figure 3.1. The calorimetric signals for chloride and nitrate exchange for 0AlFh, 12 AlFh, and 24AlFh at a) pH 5.6 and b) pH 3. An increase in voltage resulting in a positive peak corresponds to a release of energy and hence an exothermic reaction. Conversely, a decrease in voltage resulting in a negative peak corresponds to energy consumption and hence an endothermic reaction. The concentrations of each oxyanion in solutions are 0.05 M chloride and nitrate. The mass of solid used for pH 5.6 and 3 is ~ 45 mg and ~ 5 mg, respectively.

not be directly compared.

While the enthalpic sign was consistent across pHs and Al (III) contents, the magnitudes of the heats (Q_{exch}) were not. Q_{exch} increased with increasing Al and decreasing pH values. For instance, Q_{exch} for [C/N] increased from – 1.980 ± 0.1 mJ/mg for 0AlFh to -2.940 ± 0.05 for 12AlFh and -5.830 ± 0.1 mJ/mg for 24AlFh at pH 5.6 ± 0.1, and from -5.548 ± 0.1 mJ/mg for 0AlFh to -8.380 ± 0.15for 12 AlFh and -14.681 ± 0.15 mJ/mg for 24AlFh at pH 3.0 ± 0.1 (Table 3.2. See Appendix C.4 for the graph of the Q_{exch} (mJ/mg) vs Al% for various AlFhs).

Table 3.2. The heat of exchange for the representative pretreatment [C/N], the first posttreatment [C/N]

Sample	**pH**	**Q_{exch} of [C/N] (mJ/mg)**	**Q_{exch} for the first posttreatment [C/N] (mJ/mg)**	**Reduction in Q_{exch} for the first posttreatment [C/N] %**
0AlFh	5.6 (0.02)[1]	-1.98 (0.06)[2]	-1.143	42.27
12AlFh	5.6 (0.02)	-2.947 (0.02)	-0.9690	67.13
24AlFh	5.6 (0.02)	-5.083 (0.09)	-1.491	70.66
0AlFh	3 (0.03)	-5.548 (0.08)	-0.9720	82.48
12AlFh	3 (0.03)	-8.385 (0.1)	-0.5080	90.00
24AlFh	3 (0.07)	-16.59(0.2)	-0.8544	95.00

[1]*Numbers in parenthesis corresponds to the standard error*
[2]*Heats of exchange in this table are listed as negative numbers as the heat of exchange of nitrate replacing chloride was used as it is the first exchange after adsorption which can be compared with the pretreatment values.*

3.3.3 Sulfate Sorption

Figures 3.2 and 3.3 show the heat signals for continuously flowing a sulfate solution over the AlFh samples at both pH 5.6 and 3, respectively. The reaction of sulfate with the three surfaces at both pHs was exothermic and took around 50 – 60 min to reach thermal equilibrium. As evident in the figure, the exotherm for sulfate reaction with the 24 AlFh at pH 5.6 exhibited a different shape in that the initial heat evolution was followed by one occuring at a slower rate. Although not as dramatic, a slower return to baseline was also observed for the same reaction at pH 3.0.

The first solution after the sulfate treatment is NaCl and it is supposed to result in chloride replacing sulfate (a [S/C] reaction). The Cl^- endotherms following the sulfate treatment on all samples were very small and in most instances never returned to the baseline such that it was impossible to integrate them. At first glance, we would have interpreted their much smaller size relative to the sulfate peaks as an indication of a high degree of irreversibitlity in sulfate sorption.

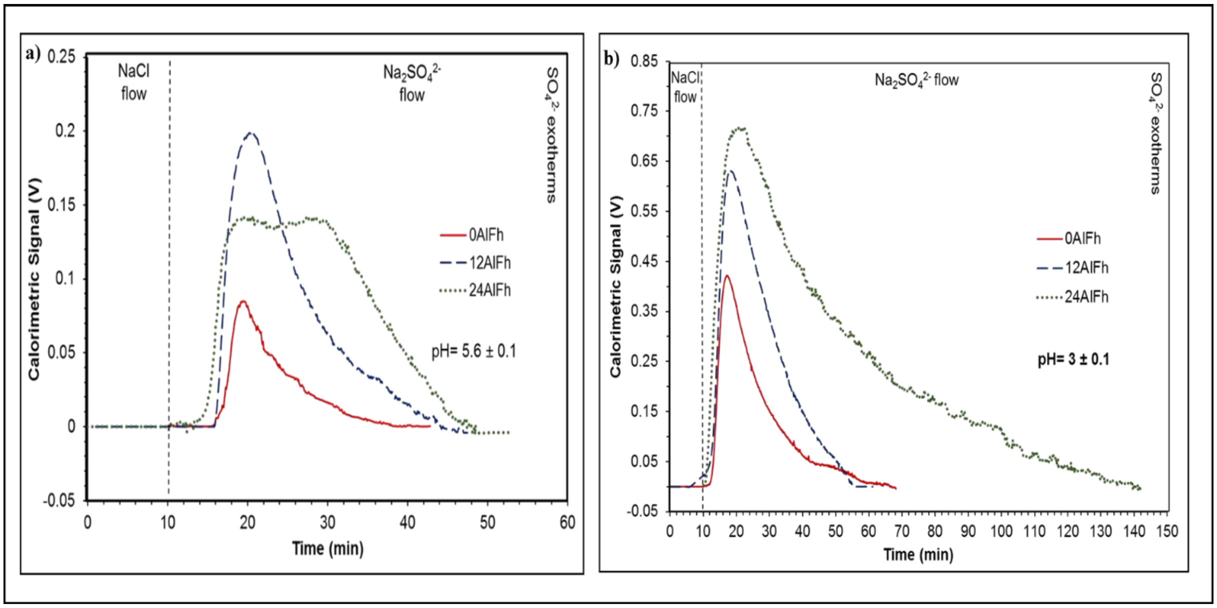

Figure 3-2. The calorimetric signal for sulfate adsorption for 0AlFh, 12 AlFh, and 24AlFh at a) pH 5.6and b) pH 3. The concentrations of sulfate is 0.005 M. The mass of solid used for pH 5.6 and 3 is ~ 45 mg and ~ 5 mg, recpectively.

However, a considerable amount of sulfate was detected in the effluent collected during this [S/C] cycle, and therefore it is hypothesized that the amounts of sulfate desorbed in this cycle correspond to a pool of sulfate complexes that are reversible to chloride. The [C/N] following the [S/C] is significantly smaller than that of the pre-sulfate treatment, and thus this pool that desorbs first to Cl represents only a fraction of the sulfate adsorbed. This will be discussed further in the next section.

The impact of Al and pH on sulfate sorption was similar to that observed on anions exchange increased as Al content increased and pH decreased. Q_{ads} values were -0.1670 mJ/mg for 0AlFh, -0.5020 mJ/mg for 12 AlFh, and -0.7410 mJ/mg for 24AlFh at pH 5.6 , and -12.32 mJ/mg for 0AlFh, -19.14 mJ/mg for 12AlFh, and -45.44 for 24 AlFh at pH 3 (Table 3.3).

Table 3.3. The heat of adsorption and enthalpy of sulfate adsorption on various AlFh and pHs

Sample ID	**pH**	**Sulfate adsorbed (μmol/mg)**	**Surface Area (m^2/g)**	**Sulfate adsorbed (μmol/m^2)**	**Energy of sulfate (mJ/mg)**	**Enthalpy (kJ/mol)**
0AlFh	5.6 (0.02)[1]	0.5610	368.0 (14)	1.545	-0.1670	-0.2970[2]
12AlFh	5.6 (0.02)	0.7450	358.0 (20)	2.052	-0.5020	-0.6740
24AlFh	5.6 (0.02)	1.007	363.0 (24)	2.774	-0.7410	-0.7360
0AlFh	3 (0.03)	5.096	368.0 (14)	14.039	-12.33	-2.280
12AlFh	3 (0.03)	6.828	358.0 (20)	18.810	-19.78	-2.897
24AlFh	3 (0.07)	12.65	363.0 (24)	34.835	-45.44	-3.617

[1]*Numbers in parenthesis corresponds to the standard error*
[2]*The enthalpy was calculated suing the heat of interaction (kJ) divided by the amount of sulfate adsorbed (mol).*

Because exposure of the 24AlFH sample to solutions at pH 3 resulted in a faint yellow effluent 4 days into the experiments which suggested possible dissolution of the solid, the experimental protocol for these conditions was slightly modified. The pH of the solutions used was gradually decreased from 3.5 to 3.2 over a period of 3 days, after which the sample was exposed to the sulfate solution at pH 3.0. This modification circumvented any solid dissolution as the effluent which was carefully monitored remained clear. Additionally, the Q_{exch} of [C/N] and [N/C] at pH 3.2 were not significantly different from those obtained at pH 3.0 prior to the solid dissolution.

The values for the mass of sulfate retained on the surface at the end of the reaction, as indicated by the return of the heat signal to the original baseline, are presented in Table 3.3. They exhibit the same trend across Al and pH values as did their corresponding Q_{ads}. Surface excess values (Γ^2) were 1.450, 1.928 and 2.534 µmol/m^2 for the 0, 12 and 24AlFh respectively at pH 5.6 and 13.06, 17.50 µmol/m^2, and 32.40for the 0, 12, and 24 AlFh respectively at pH 3.0 ± 0.1.

The enthalpy (kJ/mol) of the sulfate reaction with the AlFh's surfaces was obtained using the heat of interaction (kJ) and the amount of sulfate adsorbed (mol). The enthalpy values showed the same trends as the energies and increased with increasing Al content and decreasing pH which pointed out a fact that having more Al incorporated in the Fh and lower pH during the reaction augmented the amount of energy produced per mole of sulfate adsorbed on Fh's surface (Table 3.3).

3.3.4 Chloride and Nitrate Exchange: Post-Sulfate Treatment

The magnitude of the C/N exchange, taken as a proxy for positive surface charge, was used to assess the impact of sulfate on the positive charge and the reversibilty of sulfate adsorption. Sulfate sorption on all samples decreased the calorimetric peaks associated with both the [C/N] and [N/C] exchange as compared to the pre-sulfate peaks. This decrease indicates a loss of positive charge as sulfate sorption occurs predominantly on the same charge-bearing functional groups that are no longer "available" for ion exchange (Fig 3.3). The observed reduction in Q_{exch} was not consistent for all samples. When compared to the pre-sulfate value, the Q_{exch} for the first posttreatment [C/N] decreased by 42% for 0AlFh, 67% for 12AlFh, and 71 % for the 24AlFh samples at pH 5.6. Similarly, the decrease in Q_{exch} varied among samples at the lower pH. At pH 3, the Q_{exch} of the first postreatment [C/N] was lower by 82% for the 0AlFh, by 90% for the 12AlFh , and by 95 % for the 24AlFh samples.

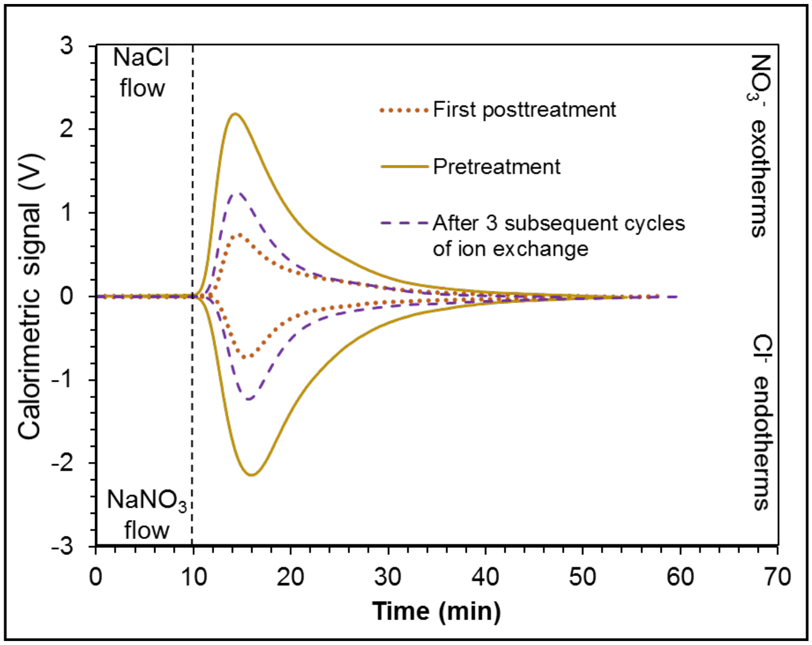

Figure 3-3. Representative calorimetric signals for [C/N] and [N/C] cycles before and after sulfate treatment. The experiment was conducted on ~ 45 mg 24AlFh at pH 5.6.

The large decrease in Q_{exch} across samples and pHs was not permanent. With subsequent C/N and N/C cycles, the peaks areas and Q_{exch} progressively increased back to stabilize at equilibrium values representing a fraction of their pre-sulfate values. These fractions were 99.03% for 0AlFh, 87.75% for 12AlFh, and 59.65 % for the 24AlFh samples at pH 5.6, and 56.031 % for 0AlFh, 53.09 % for 12AlFh, and 36.62 % for the 24AlFh samples at pH 3.0 (Table 3. 4). Therefore, the amount of the surface charge that was lost and not recovered over time or in other words the amount of sulfate that could not be desorbed from the surface increased with increasing Al content and decreasing pH.

The initial decrease and following rebound of the Q_{exch} values suggest sulfate is progressively desorbing from the surface and additional functional group sites are available to participate in C/N and N/C exchange. This desorption was further corroborated as sulfate was detected in the

Table 3.4. The heat of exchange for the representative pretreatment [C/N], the equilibrium posttreatment and the volume of solution used to reach the equilibrium posttreatment

Sample	**pH**	**Q_{exch} of [C/N] (mJ/mg)**	**Q_{exch} of equilibrium posttreatment [C/N] (mJ/mg)**	**Q_{exch} of equilibrium posttreatment [C/N] %**	**Volume of solution used to reach the equilibrium posttreatment (ml)**
0AlFh	5.6 (0.02)[1]	-1.98 (0.06)[2]	-1.960 (0.1)	99.03	746[2]
12AlFh	5.6 (0.02)	-2.947 (0.02)	-2.586 (0.02)	87.76	1695
24AlFh	5.6 (0.02)	-5.083 (0.09)	-3.032 (0.008)	59.65	1220
0AlFh	3 (0.03)	-5.548 (0.08)	-3.109 (0.03)	56.03	751
12AlFh	3 (0.03)	-8.385 (0.1)	-4.451 (0.2)	53.09	988
24AlFh	3 (0.07)	-16.59(0.2)	-6.077(0.1)	36.62	517

[1]*Numbers in parenthesis corresponds to the standard error*
[2] *the mass of solid used for pH 5.6 and 3 was ~ 45 mg and ~ 5 mg, respectively.*

effluent stream collected between the final pre-treatment C/N exchange and the last of the five post-treatment C/N and N/C cycles that did not show any further change.

In all instances, sulfate desorption was observed to be significantly slower than its adsorption and was incomplete for all samples, except for the 0AlFh sample at pH 5.6. for which the equilibrium Qexch post sulfate bounced back to 99% of its original value. Furthermore, the total volume of chloride and nitrate solutions needed to desorb the sulfate from the surface and reach these equilibrium Q_{exch} values differed between samples (Table 3.4). At pH 5.6, it took 746 mL for 0AlFh, 1695 ml for 12 AlFh and 1220 ml for 24AlFh samples for the post-exchange cycles to not show any further change. For pH 3.0, these values were 751 mL for 0AlFh, 988 mL for 12 AlFh, and 517 mL for 24AlFh samples.

3.4 DISCUSSION

3.4.1 Surface Charge

The 12AlFh and 24AlFh samples had approximately 48% and 98% more Q_{exch} than that measured for the 0AlFh at pH 5.6, and 51% and 75% more at pH 3.0. The increase in the magnitude of Q_{exch} with decreasing pH and increasing Al content indicates the surface has now significantly more surface positive charge. The shift of the pH at which the isoelectric point occurs in the 12AlFh and 24AlFH samples demonstrates that more surface hydroxyls are deprotonated at any given pH below the IEP and the number of $Fe\text{-}OH^{+1/2}$ or $Al\text{-}OH^{+1/2}$ positively surface sites is higher.

The pH at which the point of zero charge of Al minerals occurs have been reported at values ~ 9.5 – 10.0 for pure gibbsite [21, 99] and amorphous aluminum oxyhydroxides[4, 123] whereas that of Fh is consistently found to occur at lower pH values around 8.0 [11, 21]. The presence of increasing Al, appears to have given the surface charge “Aluminum-like” properties despite the fact that XRD analysis failed to detect a distinct crystalline Al hydroxide phase. In both the 12AlFh and 24AlFh samples, HRTEM-EDS revealed the Al to be homogeneously distributed across spots and particles. Neither these two results constitute definite evidence of Al (III) substitution into the Fh-structure or the lack thereof. The detection limits of both XRD and EDS analyses is around 1% or about 10,000 ppm and may miss some nanoscale heterogeneity in the composition. Previous studies of the effects of Al content on Fh structure [19, 24, 31, 101] have agreed that Al (III) substitution, as opposed to the precipitation of either distinct crystalline or amorphous Al phases, occurs up to until 20- 30 mol %, although other processes, such as Al adsorption on the surface or the possibility of nanoscale segregation of Al-rich phases that may remain undetected cannot be ruled out.

Harvey and Rhue (2008) argued that in co-precipitation environments and due to differences in solubility, Al-phases would precipitate after Fe upon NaOH addition and hence the Al is found on the surface of the Fh. While the presence of Al sorbed on the surface cannot be ruled out nor directly confirmed in our case, it is clear from our results that the presence of Al leads to more positive surface charge.

3.4.2 Sulfate Adsorption

The exothermic nature of sulfate reactions with all three samples is consistent with reported enthalpies for other oxyanions. For instance, phosphate sorption was reported to be exothermic on boehmite[80], on amorphous aluminum oxides[79] and mixed Al(III)-Fe(III) amorphous oxides [74]. Similarly, arsenate sorption on both amorphous aluminum oxides [61] and hematite nanoparticles [81] was also found to be exothermic. In contrast, and in a similar study to this one but on amorphous aluminum hydroxides, Appel et al. [79] reported sulfate adsorption to be endothermic. Their study, however, had a major difference in that the solution used to expose their sample to SO_4^{2-} was prepared in a $NaNO_3$ background instead of NaCl. Both Cl^- and NO_3^- are believed to be background electrolytes in outer-sphere complexation and are not expected, beyond regulating the ionic strength, to exert any influence on the sorption of other oxyanions particularly if it occurs in inner-sphere modes. Nevertheless, the net enthalpy measured in the flow microcalorimetry is essentially that of an exchange, and it is conceivable that the exchange, albeit fractional, of SO_4^{2-} for Cl^- be of a different enthalpic sign than that of SO_4^{2-} for NO_3^-.

While the sign of the sulfate reaction concurs to a great extent with values published, the normalized magnitudes (Q_{ads} in mJ/mg) are significantly smaller indicating a potentially weaker interaction. The increased amounts of sulfate retained at the surface with increasing Al, and decreasing pH are undoubtedly correlated to the increased surface charge measured by Q_{exch} of Cl^-

and NO_3^- and discussed above. There is not, however, a direct linear relationship between the increase in Q_{exch} and the measured Γ^2. This result is to be expected as the inner-sphere complexation of SO_4^{2-} has been reported to predominantly occur as bidentate binuclear complexes [38-39] and as such will occupy, in principle, twice as many surface sites than detected by either the Cl^- or NO_3^- probe.

The adsorption of sulfate in the presence of Al in the Fh structure appears to be kinetically slower as evidenced by the heat evolution observed for the 24 AlFh at both pHs 5.6 and 3.0. This difference can be attributed to the formation of more inner-sphere complexes which is a slower process than that of the outer-sphere formation. In their study of suflate adsorption on hematite, Wang et al. [73] measured a larger release of OH^- at a later stage of sulfate adsorption. Given that OH^- release in an indication of inner-sphere formation, the authors concluded that this process was happening after the intial rapid stage of adsorption that occurred without OH^- release. This early stage is hence domimated by outer-sphere complexation.

3.4.3 Sulfate Desorption and Reversibility

In this work, the sulfate desorption has been loosely classified into three pools based on the kinetics of their reversibility to chloride and nitrate: fast reversible, slow reversible and irreversible. In contrast to sulfate, Cl^- and NO_3^- reactions with all three AlFh surfaces were reversible, and the rates of their adsorption and desorption were equal. After flushing the surface, for instance with nitrate, all the chloride injected in the previous step would be released, and both anion peaks show identical Q_{exch} values. If this reasoning is applied to sulfate desorption, the amount of sulfate recovered in the effluent during the first [S/C] can be assigned to the fast reversible pool. The almost negligible Q_{exch} associated with the desorption of this pool may be attributed to two factors: very small ΔH values of [S/C] exchange or a very small fraction of this reversible pool. The slow reversible pool corresponds to the sulfate that was progressively flushed off the surface between the first posttreatment [C/N] and the last of the five post-treatment C/N and N/C cycles that did not show any further change. The desorption of the pool was evidenced by the progressive bouncing back of the Q_{exch}. The remaining sulfate on the surface beyond this point is considered irreversible to Cl^- and NO_3^- regardless of the numbers of C/N cycles and cumulative volume passed through the column. The distribution of the three fractions appears to be impacted by both the Al content and pH values (Figure 3.4). Overall, increasing Al content and decreasing pH seems to increase the fractions of the irreversible pool. Sulfate is known to form both outer- and inner-sphere complexes on Fh [19, 38-40], hematite[55, 73, 115, 124-125] and aluminum oxides[79]. In this study, a qualitative correspondence can be made between the outer-sphere and fast irreversible pools and inner-sphere complexes with slow irreversible (inverse relation) and reversible pools (direct relation).

By putting all the results together, we hypothesize that an increase in Al content and a decrease in pH lead to a larger fraction of inner-sphere bidentate complexes which tend to be more irreversible and produces higher Q_{ads} and a smaller fraction of outer-sphere complexes that can be reversed quickly. The desorption of inner-sphere complexes has been indeed reported to be a slower process compared to that of outer-sphere [69, 74, 79-80].

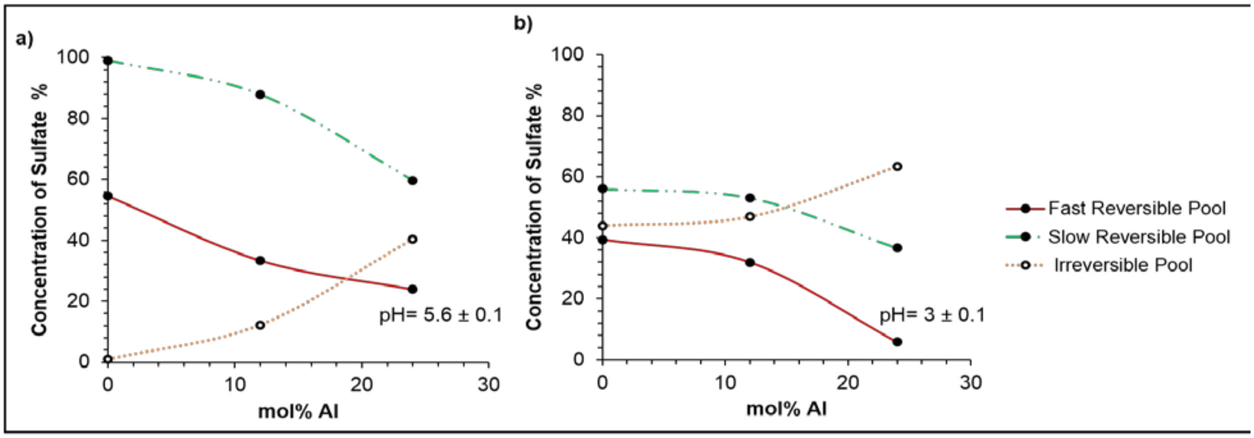

Figure 3.4. Qualitative estimation of the variation in reversibility of sulfate desorption with Al concentration and pH. The values for the fast reversible pool were calculated based on the amount of sulfate measured in the effluent during the C/S. The values of slow reversible pool correspond to the Q_{exch} (%) of the equilibrium post-treatment, and the values of the irreversible pool were calculated based on the amount Q_{exch} (%) lost after reaching equilibrium posttreatment.

A decrease in pH, from 5.6 to 3.0 leads to a significantly higher density of positively charged surface sites, a higher density of >Fe-OH$^{+1/2}$ and possibly Al-OH$^{+1/2}$ sites, and lower amount of hydration which in all cases favor the adsorption of sulfate[39, 99]. Conversely, as pH increases the density of >Fe-OH and Fe-O- become predominant suppressing the ligand exchange (i.e., inner-sphere complexation). Under higher pH conditions, sulfate complexation with H_2O surface functional groups (i.e., outer-sphere complexation) is more favorable than ligand exchange since more energy is required to break >Fe-OH bond comparing with weaker >Fe-OH$_2$ bond[19, 38-39, 126]. Although outer-sphere complexation is more sensitive to changes in surface charge than inner-sphere, as pH increases, inner-sphere adsorption is suppressed since it cannot compete with outer-sphere resulting in the dominance of outer-sphere complexation at higher pH. Finally, as pH approaches the point of zero charge, outer-sphere complexation would also be gradually disfavored as the surfaces become less positively charged[39].

The incorporation of Al (III) into Fh structure increases the disorder of its structure and thus changing the number of positive charges on the surface is not the only consequence of this substitution. According to Hiemstra and Van Riemsdijk [10] and Hiemstra [11], the 0 0 1 face of Fh favors inner-sphere complexation as it contains singly coordinated surface groups with the sequence of adjacent edge-sharing octahedra which are believed to increase as defects are increased in the Fh structure.

Cismasu et al. [18] also found Al substituted in the Fh structure in octahedral coordination by oxygen to be conducive to binuclear bidentate complexes for oxyanions. Thus, with enhancing Al %, besides increasing positive surface sites, the defect in the structure of Fh causes increased numbers of singly coordinated surface groups, that is, the surface structure of Fh changes such that the more inner-sphere complexation of sulfate is favored.

3.5 Conclusion

This work used flow microcalorimetry to study the role of aluminum substitution on the interaction energy of chloride (Cl^-) and nitrate (NO_3^-), and adsorption of sulfate (SO_4^{2-}) onto Fh. The energetics and reversibility of sulfate adsorption/desorption on some aluminum ferrihydrites indicated that anion exchange on Fh surface is strongly correlated to the concentration of Al and pH. Increasing Al and decreasing pH increased the heat of exchange of chloride, nitrate, and heat of adsorption of sulfate on the Fh surface and sulfate adsorption. The post-sulfate treatment experiment showed the same trend for the percentage reduction in the Q_{exch} of the first posttreatment [C/N] which decreased at higher Al concentration and lower pH. A classification for different sulfate desorption behaviors was proposed in this work consisting of different pools, reversible attributed to outer-sphere complexation, and slow irreversible and absolute irreversible which correspond to inner-sphere complexation. At higher Al concentration and lower pH, the irreversible pools (inner-sphere complexes) were dominant, while with increasing pH and decreasing Al, the reversible pool (outer-sphere) is favored. Increasing Al concentrations raises the pH_{iep}, and the defects in Fh structure provides a higher density of positive surface sites and singly coordinated surface groups which favor inner-sphere complexation.

Overall, a systematic study of the sulfate adsorption/desorption helps to understand the fate and transport of oxyanions, toxic metal(loid)s, and other contaminants. This work showed that the different chemical compositions of minerals and oxyanions in natural environments impact on the adsorption/ desorption of sulfate on Fh as as Al and more acidic pH promoted the chemical interaction of sulfate with Fh.

4 CONCLUSIONS

Flow microcalorimetry was used in this work to measure the energetics and reversibility of oxyanion adsorption/desorption on ferrihydrite. Also, from the oxyanions studied, sulfate was chosen as a probe to investigate the role of aluminum substitution on oxyanion complexation by Fh to obtain systematic insight into oxyanion-ferrihydrite interface interactions in the natural environment.

Chapter 2 aimed to systematically measure the heat of exchange, molar enthalpy, and adsorption reversibility of oxyanions that are known to form both outer-sphere and inner-sphere complexes on ferrihydrite (Fh). Fh is one of the most reactive poorly crystalline iron (hydr) oxides pervasive in soil and groundwater with the high specific surface area and high density of reactive surface sites. Chloride, nitrate, sulfate, phosphate, and arsenate were chosen since they were previously reported to form a wide range of surface complexes ranging from electrostatic outer-sphere to various inner-sphere complexes.

The calorimetric signal for each oxyanion interacting with the Fh surface was found to be exothermic, while the reaction for chloride replacing nitrate was endothermic. The heat of exchange (Q_{exch}), reaction times, and peak areas for [C/N] and [N/C] were similar, while these parameters showed considerable variability for the other oxyanions. Arsenate had the highest measured Q_{ads} followed by phosphate and sulfate. The reversibility of oxyanion adsorption was also examined. Chloride and nitrate were completely reversible, while 99 % of the sulfate, 50.7% of phosphate and 44.4 % arsenate were desorbed after conducting several subsequent C/N and N/C cycles indicating a higher fraction of irreversible complexes for these oxyanions.

The molar enthalpies (ΔH_{ads}) of oxyanion adsorption increased following a positive Hofmeister series and mirrored the strength and complexations mode reported for each oxyanion, such that $\Delta H_{Cl^-} = \Delta H_{NO_3^-} < \Delta H_{SO_4^{2-}} < \Delta H_{PO_4^-} < \Delta H_{AsO_4^{2-}}$. Based on the results, the bidentate inner-sphere complexes of arsenate exhibited the highest ΔH_{ads}, followed by a mixture of monodentate/bidentate complexes for phosphate, a mixture of outer-sphere/inner-sphere complexes for sulfate, and entirely outer-sphere complexes for nitrate and chloride.

In Chapter 3, sulfate was used as a probe to study the effect of Al-substitution on the sorptive capacity of ferrihydrite. Three different Al-substituted ferrihydrite were synthesized, and the energetics and reversibility of sulfate adsorption and desorption and heat of exchange of chloride and nitrate were determined to gain a mechanistic insight into oxyanion AlFh interface interactions. The concentration of Al (III) incorporated into Fh and pH were directly correlated with the heat of exchange and adsorption of anions on Fh surface such that the Q_{exch} of chloride and nitrate, and the heat of adsorption of sulfate increased with increasing Al and decreasing pH.

The reduction in the Q_{exch} of the first post-treatment [C/N] exhibited the same trend as it decreased with increased Al concentration and at lower pH. This reduction suggested that the surface of Fh is blocked with sulfate which occupies the functional groups and no further surface is available for ion exchange. The heat of exchange was recovered with conducting more subsequent C/N and N/C cycles which stabilized at equilibrium values representing a fraction of their pre-sulfate values. The percentage of the heat of exchange recovered were different across the samples and also increased with increasing Al content and decreasing pH.

Based on the different behaviors of sulfate desorbing from the various AlFhs at two different pHs, a classification was proposed in this work in that three pools were identified for the reversibility of sulfate, fast reversible, slow reversible and irreversible. We suggest that the different pools correspond to the type of sulfate complexes on the Fh surface in that outer-sphere corresponds to fast irreversible pools, and inner-sphere complexes are attributed to slow reversible and irreversible pools. Similar to decreasing pH, increasing the Al (III) concentration provides more positive surface charge for sulfate adsorption as evidenced by increasing pH_{iep} values. Also, with more Al concentration, defects in the Fh structure increase providing more singly coordinated surface groups which promote inner-sphere complexation. Overall, the slow reversible and irreversible pools (inner-sphere complexes) were dominant at lower pH and higher Al concentration, while with increasing pH and decreasing Al, the fast reversible pool (outer-sphere) is favored.

Overall, a systematic study of oxyanion adsorption on minerals and poorly crystalline minerals such as Fh is of critical importance to gain insights into the fate and transport of oxyanions, toxic metal(loid)s and other contaminants. This work showed that the oxyanions do not exhibit the same behavior during adsorption/desorption reactions. Also, it has been proved that different chemical conditions impact on the interaction of oxyanions with absorbents as Al and more acidic pH strengthen the chemical interactions of oxyanions with Fh with the substantial increase in the relative proportion of inner-sphere surface complexes.

4.1 Future Work

To our understanding, this work was the first to study the energetics and reversibility of a wide range of oxyanions adsorption/desorption on Fh which is known as a highly reactive and poorly crystalline mineral. In the future the results obtained in this work will be complemented with some other techniques such as differential pair distribution function (d-PDF) analysis to quantify the fraction of outer-sphere/inner-sphere complexes of sulfate and also other oxyanions of interest on Fh and AlFh. In d-PDF analysis the Fourier transform of Bragg and diffuse scattering is taken to obtain a real space distribution of pairs of atoms in a structure which is proved powerful in solids [44].

PDF analysis involves taking the Fourier transform of the total structure function (both the Bragg and diffuse scattering), yielding a real space distribution of distances between pairs of atoms in a structure weighted by the scattering power of the atoms responsible for the peak. D-PDF is an ideal complementary technique to FAMC in that i) both techniques can obtain data in situ from flowing liquids, which is more realistic to environmental conditions, and 2) d-PDF is sensitive to the local environments of lower-Z elements such as S and Al, which can be challenging to probe by techniques such as EXAFS. Combining FAMC and d-PDF will lead to a new understanding of oxyanion interactions with pure Fh and AlFh and the mechanism by which Al, and potentially other impurities, change the reactivity of FH in natural environments.

REFERENCES

1. Sposito, G. The Chemistry of Soils. Oxford University Press: New York :, 1987.
2. Chorover, J.; Brusseau, M. L. Kinetics of Sorption—Desorption. In Kinetics of Water-Rock Interaction, Brantley, S. L.; Kubicki, J. D.; White, A. F., Eds. Springer New York: New York, NY, 2008; pp 109-149.
3. Sparks, D. L. Environmental Soil Chemistry. 2nd ed; San Diego, Calif. : London :, 2003.
4. McBride, M. B. Environmental Chemistry of Soils. New York : Oxford University Press, 1994.
5. Stollenwerk, K. G. Geochemical Processes Controlling Transport of Arsenic in Groundwater: A Review of Adsorption. In Arsenic in Ground Water: Geochemistry and Occurrence, Welch, A. H.; Stollenwerk, K. G., Eds. Springer US: Boston, MA, 2003; pp 67-100.
6. Hochella, M. F.; Lower, S. K.; Maurice, P. A.; Penn, R. L.; Sahai, N.; Sparks, D. L.; Twining, B. S. Nanominerals, Mineral Nanoparticles, and Earth Systems. *Science* **2008,** 319 (5870), 1631.
7. Jentzsch, T. L.; Penn, R. L. Influence of Aluminum Doping on Ferrihydrite Nanoparticle Reactivity. *J. Phys. Chem. B* **2006,** 110 (24), 11746.
8. Cornell, R. M.; Schwertmann, U. The Iron Oxides : Structure, Properties, Reactions, Occurences and Uses. 2., compl. rev. and ext. ed. ed.; Wiley-VCH: Weinheim :, 2003.
9. Michel, F. M.; Ehm, L.; Antao, S. M.; Lee, P. L.; Chupas, P. J.; Liu, G.; Strongin, D. R.; Schoonen, M. A. A.; Phillips, B. L.; Parise, J. B. The Structure of Ferrihydrite, a Nanocrystalline Material. *Science* **2007,** 316 (5832), 1726.
10. Hiemstra, T.; Van Riemsdijk, W. H. A Surface Structural Model for Ferrihydrite I: Sites Related to Primary Charge, Molar Mass, and Mass Density. *Geochimica et Cosmochimica Acta* **2009,** 73 (15), 4423-4436.
11. Hiemstra, T. Surface and Mineral Structure of Ferrihydrite. *Geochimica et Cosmochimica Acta* **2013,** 105, 316-325.
12. Villalobos, M.; Antelo, J. A Unified Surface Stuctural Model for Ferrihydrite: Proton Charge, Electrolyte Binding, and Arsenate Adsorption. *Revista internacional de contaminación ambiental* **2011**, 27 (2) 139-151.
13. Harrington, R.; Hausner, D. B.; Xu, W.; Bhandari, N.; Michel, F. M.; Brown, G. E.; Strongin, D. R.; Parise, J. B. Neutron Pair Distribution Function Study of Two-Line Ferrihydrite. *Environmental Science & Technology* **2011,** 45 (23), 9883-9890.
14. Manceau, A. Critical Evaluation of the Revised Akdalaite Model for Ferrihydrite. *American Mineralogist* **2011,** 96 (4), 521.
15. Drits, V. A.; Sakharov, B. A.; Salyn, A. L.; Manceau, A. Structural Model for Ferrihydrite. *Clay Minerals* **1993,** 28 (2), 185.
16. Michel, F. M.; Barrón, V.; Torrent, J.; Morales, M. P.; Serna, C. J.; Boily, J. F.; Liu, Q.; Ambrosini, A.; Cismasu, A. C.; Brown, G. E. Ordered Ferrimagnetic Form of Ferrihydrite Reveals Links among Structure, Composition, and Magnetism. *Proc. Natl. Acad. Sci. U. S. A.* **2010,** 107 (7), 2787.
17. Chadwick, J.; Jones, D. H.; Thomas, M. F.; Tatlock, G. J.; Devenish, R. W. A Mössbauer Study of Ferrihydrite and Aluminium Substituted Ferrihydrites. *Journal of Magnetism and Magnetic Materials* **1986,** 61 (1), 88-100.

18. Cismasu, A. C.; Michel, F. M.; Stebbins, J. F.; Levard, C.; Brown Jr, G. E. Properties of Impurity-Bearing Ferrihydrite I. Effects of Al Content and Precipitation Rate on the Structure of 2-Line Ferrihydrite. *Geochimica et Cosmochimica Acta* **2012,** 92, 275-291.
19. Johnston, C. P.; Chrysochoou, M. Mechanisms of Chromate, Selenate, and Sulfate Adsorption on Al-Substituted Ferrihydrite: Implications for Ferrihydrite Surface Structure and Reactivity. *Environmental Science & Technology* **2016,** 50 (7), 3589-3596.
20. Cismasu, A. C.; Michel, F. M.; Tcaciuc, A. P.; Brown Jr, G. E. Properties of Impurity-Bearing Ferrihydrite Iii. Effects of Si on the Structure of 2-Line Ferrihydrite. *Geochimica et Cosmochimica Acta* **2014,** 133, 168-185.
21. Cismasu, A. C.; Levard, C.; Michel, F. M.; Brown Jr, G. E. Properties of Impurity-Bearing Ferrihydrite Ii: Insights into the Surface Structure and Composition of Pure, Al- and Si-Bearing Ferrihydrite from Zn(Ii) Sorption Experiments and Zn K-Edge X-Ray Absorption Spectroscopy. *Geochimica et Cosmochimica Acta* **2013,** 119, 46-60.
22. Cornell, R. M.; Schwertmann, U. Sources of Figures and Tables
the Iron Oxides. 2004; p 659-664.
23. Liu, Y.-T.; Hesterberg, D. Phosphate Bonding on Noncrystalline Al/Fe-Hydroxide Coprecipitates. *Environmental Science & Technology* **2011,** 45 (15), 6283-6289.
24. Massey, M. S.; Lezama-Pacheco, J. S.; Michel, F. M.; Fendorf, S. Uranium Incorporation into Aluminum-Substituted Ferrihydrite During Iron(Ii)-Induced Transformation. *Environmental Science: Processes & Impacts* **2014,** 16 (9), 2137-2144.
25. Adra, A.; Morin, G.; Ona-Nguema, G.; Brest, J. Arsenate and Arsenite Adsorption onto Al-Containing Ferrihydrites. Implications for Arsenic Immobilization after Neutralization of Acid Mine Drainage. *Appl. Geochem.* **2015,** 64, 2.
26. Bazilevskaya, E.; Archibald, D. D.; Aryanpour, M.; Kubicki, J. D.; Martínez, C. E. Aluminum Coprecipitates with Fe (Hydr) Oxides: Does Isomorphous Substitution of Al 3 for Fe 3 in Goethite Occur? *Geochim. Cosmochim. Acta* **2011,** 75 (16), 4667.
27. Ekstrom, E. B.; Learman, D. R.; Madden, A. S.; Hansel, C. M. Contrasting Effects of Al Substitution on Microbial Reduction of Fe (Iii) (Hydr) Oxides. *Geochim. Cosmochim. Acta* **2010,** 74 (24), 7086.
28. Hansel, C. M.; Learman, D. R.; Lentini, C. J.; Ekstrom, E. B. Effect of Adsorbed and Substituted Al on Fe(Ii)-Induced Mineralization Pathways of Ferrihydrite. *Geochimica et Cosmochimica Acta* **2011,** 75 (16), 4653-4666.
29. Hu, Y.; Li, Q.; Lee, B.; Jun, Y. Aluminum Affects Heterogeneous Fe (Iii) (Hydr) Oxide Nucleation, Growth, and Ostwald Ripening. *Environ. Sci. Technol.* **2013,** 48 (1), 299.
30. Latta, D. E.; Bachman, J. E.; Scherer, M. M. Fe Electron Transfer and Atom Exchange in Goethite: Influence of Al-Substitution and Anion Sorption. *Environ. Sci. Technol.* **2012,** 46 (19), 10614.
31. Manceau, A.; Gates, W. P. Incorporation of Al in Iron Oxyhydroxides: Implications for the Structure of Ferrihydrite. *Clay Minerals* **2013,** 48 (3), 481-489.
32. Cismasu, A. C.; Levard, C.; Michel, F. M.; Brown, G. E. Properties of Impurity-Bearing Ferrihydrite Ii: Insights into the Surface Structure and Composition of Pure, Al-and Si-Bearing Ferrihydrite from Zn (Ii) Sorption Experiments and Zn K-Edge X-Ray Absorption Spectroscopy. *Geochim. Cosmochim. Acta* **2013,** 119, 46.
33. Manceau, A.; Gates, W. Incorporation of Al in Iron Oxyhydroxides: Implications for the Structure of Ferrihydrite. *Clay Miner.* **2013,** 48 (3), 481.

34. Sorptive Interaction of Oxyanions with Iron Oxides: A Review. *Polish Journal of Environmental Studies* **2013,** 22 (1), 7-24.
35. Kafkafi, U. In Oxyanion Sorption on Soil Surfaces, Berlin, Heidelberg, Springer Berlin Heidelberg: Berlin, Heidelberg, 1989; pp 33-42.
36. Sposito, G. The Chemistry of Soils. 2nd ed. ed.; Oxford University Press: Oxford ;, 2008.
37. Kabengi, N. J.; Rhue, R. D.; Daroub, S. H. Using Flow Calorimetry to Determine the Molar Heats of Cation and Anion Exchange and the Point of Zero Net Charge on Amorphous Aluminum Hydroxides. *Soil Science* **2006,** 171 (1), 13-20.
38. Zhu, M.; Northrup, P.; Shi, C.; Billinge, S. J.; Sparks, D. L.; Waychunas, G. A. Structure of Sulfate Adsorption Complexes on Ferrihydrite. *Environ. Sci. Technol. Lett.* **2014,** 1 (1), 97.
39. Gu, C.; Wang, Z.; Kubicki, J. D.; Wang, X.; Zhu, M. X-Ray Absorption Spectroscopic Quantification and Speciation Modeling of Sulfate Adsorption on Ferrihydrite Surfaces. *Environmental Science & Technology* **2016,** 50 (15), 8067-8076.
40. Hinkle, M. A. G.; Wang, Z.; Giammar, D. E.; Catalano, J. G. Interaction of Fe(Ii) with Phosphate and Sulfate on Iron Oxide Surfaces. *Geochim. Cosmochim. Acta* **2015,** 158, 130.
41. Antelo, J.; Fiol, S.; Pérez, C.; Mariño, S.; Arce, F.; Gondar, D.; López, R. Analysis of Phosphate Adsorption onto Ferrihydrite Using the Cd-Music Model. *Journal of Colloid and Interface Science* **2010,** 347 (1), 112-119.
42. Antelo, J.; Arce, F.; Fiol, S. Arsenate and Phosphate Adsorption on Ferrihydrite Nanoparticles. Synergetic Interaction with Calcium Ions. *Chemical Geology* **2015,** 410, 53-62.
43. Arai, Y.; Sparks, D. L. Atr–Ftir Spectroscopic Investigation on Phosphate Adsorption Mechanisms at the Ferrihydrite–Water Interface. *Journal of Colloid and Interface Science* **2001,** 241 (2), 317-326.
44. Harrington, R.; Hausner, D. B.; Bhandari, N.; Strongin, D. R.; Chapman, K. W.; Chupas, P. J.; Middlemiss, D. S.; Grey, C. P.; Parise, J. B. Investigation of Surface Structures by Powder Diffraction: A Differential Pair Distribution Function Study on Arsenate Sorption on Ferrihydrite. *Inorganic Chemistry* **2010,** 49 (1), 325-330.
45. Fakhreddine, S.; Dittmar, J.; Phipps, D.; Dadakis, J.; Fendorf, S. Geochemical Triggers of Arsenic Mobilization During Managed Aquifer Recharge. *Environmental Science & Technology* **2015,** 49 (13), 7802-7809.
46. Violante, A.; Pigna, M. Competitive Sorption of Arsenate and Phosphate on Different Clay Minerals and Soils. *Soil Science Society of America Journal* **2002,** 66 (6), 1788-1796.
47. Fendorf, S.; Eick, M. J.; Grossl, P.; Sparks, D. L. Arsenate and Chromate Retention Mechanisms on Goethite. 1. Surface Structure. *Environ. Sci. Technol.* **1997,** 31 (2), 315.
48. McAuley, B.; Cabaniss, S. E. Quantitative Detection of Aqueous Arsenic and Other Oxoanions Using Attenuated Total Reflectance Infrared Spectroscopy Utilizing Iron Oxide Coated Internal Reflection Elements to Enhance the Limits of Detection. *Analytica Chimica Acta* **2007,** 581 (2), 309-317.
49. Oze, C.; Bird, D. K.; Fendorf, S. Genesis of Hexavalent Chromium from Natural Sources in Soil and Groundwater. *Proc. Natl. Acad. Sci. U. S. A.* **2007,** 104 (16), 6544.
50. Manning, B. A.; Fendorf, S. E.; Suarez, D. L. Arsenic(Iii) Complexation and Oxidation Reactions on Soil. In Biogeochemistry of Environmentally Important Trace Elements, American Chemical Society: 2002; Vol. 835, pp 57-69.
51. Manning, B. A.; Goldberg, S. Modeling Competitive Adsorption of Arsenate with Phosphate and Molybdate on Oxide Minerals. *Soil Science Society of America Journal* **1996,** 60, 121-131.

52. Gao, Y.; Mucci, A. Individual and Competitive Adsorption of Phosphate and Arsenate on Goethite in Artificial Seawater. *Chemical Geology* **2003,** 199 (1), 91-109.
53. Kubicki, J. D.; Paul, K. W.; Kabalan, L.; Zhu, Q.; Mrozik, M. K.; Aryanpour, M.; Pierre-Louis, A. M.; Strongin, D. R. Atr–Ftir and Density Functional Theory Study of the Structures, Energetics, and Vibrational Spectra of Phosphate Adsorbed onto Goethite. *Langmuir* **2012,** 28 (41), 14573.
54. Brady, N. C.; Weil, R. R. The Nature and Properties of Soils. Fifteenth edition. ed.; Pearson: Boston :, 2017.
55. Hug, S. J. In Situ Fourier Transform Infrared Measurements of Sulfate Adsorption on Hematite in Aqueous Solutions. *J. Colloid Interface Sci.* **1997,** 188 (2), 415.
56. Crawford, N. M.; Glass, A. D. M. Molecular and Physiological Aspects of Nitrate Uptake in Plants. *Trends in Plant Science* **1998,** 3 (10), 389-395.
57. von Wirén, N.; Gazzarrini, S.; Frommer, W. B. Regulation of Mineral Nitrogen Uptake in Plants. *Plant and Soil* **1997,** 196 (2), 191-199.
58. Crawford, N. M. Nitrate: Nutrient and Signal for Plant Growth. *The Plant Cell* **1995,** 7 (7), 859-868.
59. Loganathan, P.; Vigneswaran, S.; Kandasamy, J. Enhanced Removal of Nitrate from Water Using Surface Modification of Adsorbents – a Review. *Journal of Environmental Management* **2013,** 131, 363-374.
60. Katou, H. Determining Competitive Nitrate and Chloride Adsorption in an Andisol by the Unsaturated Transient Flow Method. *Soil Science and Plant Nutrition* **2004,** 50 (1), 119-127.
61. Kabengi, N. J.; Daroub, S. H.; Rhue, R. D. Energetics of Arsenate Sorption on Amorphous Aluminum Hydroxides Studied Using Flow Adsorption Calorimetry. *Journal of Colloid and Interface Science* **2006,** 297 (1), 86-94.
62. White, P. J.; Broadley, M. R. Chloride in Soils and Its Uptake and Movement within the Plant: A Review. *Annals of Botany* **2001,** 88 (6), 967-988.
63. Liittge, A.; Arvidson, R. S. The Mineral-Water Interface. In Kinetics of Water-Rock Interaction, Brantley, S. L.; Kubicki, J. D.; White, A. F., Eds. Springer New York: New York, NY, 2008; pp 73-107.
64. Brantley, S. L. Kinetics of Mineral Dissolution. In Kinetics of Water-Rock Interaction, Brantley, S. L.; Kubicki, J. D.; White, A. F., Eds. Springer New York: New York, NY, 2008; pp 151-210.
65. Benning, L. G.; Waychunas, G. A. Nucleation, Growth, and Aggregation of Mineral Phases: Mechanisms and Kinetic Controls. In Kinetics of Water-Rock Interaction, Brantley, S. L.; Kubicki, J. D.; White, A. F., Eds. Springer New York: New York, NY, 2008; pp 259-333.
66. Steefel, C. I. Geochemical Kinetics and Transport. In Kinetics of Water-Rock Interaction, Brantley, S. L.; Kubicki, J. D.; White, A. F., Eds. Springer New York: New York, NY, 2008; pp 545-589.
67. Fukushi, K.; Aoyama, K.; Yang, C.; Kitadai, N.; Nakashima, S. Surface Complexation Modeling for Sulfate Adsorption on Ferrihydrite Consistent with in Situ Infrared Spectroscopic Observations. *Appl. Geochem.* **2013,** 36, 92.
68. Fukushi, K.; Sverjensky, D. A. A Surface Complexation Model for Sulfate and Selenate on Iron Oxides Consistent with Spectroscopic and Theoretical Molecular Evidence. *Geochim. Cosmochim. Acta* **2007,** 71 (1), 1.

69. Kabengi, N. J.; Chrysochoou, M.; Bompoti, N.; Kubicki, J. D. An Integrated Flow Microcalorimetry, Infrared Spectroscopy and Density Functional Theory Approach to the Study of Chromate Complexation on Hematite and Ferrihdyrite. *Chemical Geology* **2017,** 464, 23-33.
70. Manceau, A.; Charlet, L. The Mechanism of Selenate Adsorption on Goethite and Hydrous Ferric Oxide. *Journal of Colloid and Interface Science* **1994,** 168 (1), 87-93.
71. Peak, D.; Ford, R. G.; Sparks, D. L. An in Situ Atr-Ftir Investigation of Sulfate Bonding Mechanisms on Goethite. *J. Colloid Interface Sci.* **1999,** 218 (1), 289.
72. Tian, L.; Shi, Z.; Lu, Y.; Dohnalkova, A. C.; Lin, Z.; Dang, Z. Kinetics of Cation and Oxyanion Adsorption and Desorption on Ferrihydrite: Roles of Ferrihydrite Binding Sites and a Unified Model. *Environmental Science & Technology* **2017,** 51 (18), 10605-10614.
73. Wang, X.; Wang, Z.; Peak, D.; Tang, Y.; Feng, X.; Zhu, M. Quantification of Coexisting Inner- and Outer-Sphere Complexation of Sulfate on Hematite Surfaces. *ACS Earth and Space Chemistry* **2018,** 2 (4), 387-398.
74. Harvey, O. R.; Rhue, R. D. Kinetics and Energetics of Phosphate Sorption in a Multi-Component Al(Iii)–Fe(Iii) Hydr(Oxide) Sorbent System. *Journal of Colloid and Interface Science* **2008,** 322 (2), 384-393.
75. A., M. M.; A., F. R.; R., H. I. Mechanism of Phosphate Interaction with Two Reference Clays and an Anatase Pigment. *Journal of Chemical Technology & Biotechnology* **1993,** 58 (4), 387-389.
76. CHIEN, S. H.; SAVANT, N. K.; MOKWUNYE, U. Effect of Temperature on Phosphate Sorption and Desorption in Two Acid Soils. *Soil Science* **1982,** 133 (3), 160-166.
77. J., B. N. The Description of Desorption of Phosphate from Soil. *Journal of Soil Science* **1979,** 30 (2), 259-270.
78. N., F. P. Kinetic Control of Dissolved Phosphate in Natural Rivers and Estuaries: A Primer on the Phosphate Buffer Mechanism1. *Limnology and Oceanography* **1988,** 33 (4part2), 649-668.
79. Appel, C.; Rhue, D.; Kabengi, N.; Harris, W. Calorimetric Investigation of the Nature of Sulfate and Phosphate Sorption on Amorphous Aluminum Hydroxide. *Soil Science* **2013,** 178 (4), 180-188.
80. Adrian Gale, S.; Harvey, O. R.; Dean Rhue, R. Phosphate Alteration of Chloride Behavior at the Boehmite–Water Interface: New Insights from Ion-Probe Flow Adsorption Microcalorimetry. *Journal of Colloid and Interface Science* **2015,** 455, 71-77.
81. Sabur, M. A.; Goldberg, S.; Gale, A.; Kabengi, N.; Al-Abadleh, H. A. Temperature-Dependent Infrared and Calorimetric Studies on Arsenicals Adsorption from Solution to Hematite Nanoparticles. *Langmuir* **2015,** 31 (9), 2749-2760.
82. Situm, A.; Rahman, M. A.; Allen, N.; Kabengi, N.; Al-Abadleh, H. A. Atr-Ftir and Flow Microcalorimetry Studies on the Initial Binding Kinetics of Arsenicals at the Organic–Hematite Interface. *The Journal of Physical Chemistry A* **2017,** 121 (30), 5569-5579.
83. Schwertmann, U. B. B. R. D.; Cornell, R. M. Iron Oxides in the Laboratory Preparation and Characterization. Second, completely rev. and extended ed. ed.; Wiley-VCH: Weinheim :, 2000. Volltext http://sfx.ethz.ch/sfx_locater?sid=ALEPH:EBI01&genre=book&isbn=9783527296699.
84. Rhue, R. D.; Appel, C.; Kabengi, N. Measuring Surface Chemical Properties of Soil Using Flow Calorimetry 1. *Soil Science* **2002,** 167 (12), 782-790.
85. Machesky, M. L.; Bischoff, B. L.; Anderson, M. A. Calorimetric Investigation of Anion Adsorption onto Goethite. *Environmental Science & Technology* **1989,** 23 (5), 580-587.

86. Morin, G.; Ona-Nguema, G.; Wang, Y.; Menguy, N.; Juillot, F.; Proux, O.; Guyot, F.; Calas, G.; Brown Jr, G. E. Extended X-Ray Absorption Fine Structure Analysis of Arsenite and Arsenate Adsorption on Maghemite. *Environmental Science & Technology* **2008,** 42 (7), 2361-2366.
87. Elzinga, E. J.; Sparks, D. L. Phosphate Adsorption onto Hematite: An in Situ Atr-Ftir Investigation of the Effects of Ph and Loading Level on the Mode of Phosphate Surface Complexation. *Journal of Colloid and Interface Science* **2007,** 308 (1), 53-70.
88. Elzinga, E. J.; Kretzschmar, R. In Situ Atr-Ftir Spectroscopic Analysis of the Co-Adsorption of Orthophosphate and Cd(Ii) onto Hematite. *Geochimica et Cosmochimica Acta* **2013,** 117, 53-64.
89. Hiemstra, T. Formation, Stability, and Solubility of Metal Oxide Nanoparticles: Surface Entropy, Enthalpy, and Free Energy of Ferrihydrite. *Geochimica et Cosmochimica Acta* **2015,** 158, 179-198.
90. Jambor, J. L.; Dutrizac, J. E. Occurrence and Constitution of Natural and Synthetic Ferrihydrite, a Widespread Iron Oxyhydroxide. *Chemical Reviews* **1998,** 98 (7), 2549-2586.
91. Ridley, M. K.; Hiemstra, T.; van Riemsdijk, W. H.; Machesky, M. L. Inner-Sphere Complexation of Cations at the Rutile–Water Interface: A Concise Surface Structural Interpretation with the Cd and Music Model. *Geochimica et Cosmochimica Acta* **2009,** 73 (7), 1841-1856.
92. Rancourt, D. G.; Meunier, J. F. Constraints on Structural Models of Ferrihydrite as a Nanocrystalline Material. *American Mineralogist* **2008,** 93 (8-9), 1412.
93. Hiemstra, T.; Riemsdijk, W. H. V.; Rossberg, A.; Ulrich, K.-U. A Surface Structural Model for Ferrihydrite Ii: Adsorption of Uranyl and Carbonate. *Geochimica et Cosmochimica Acta* **2009,** 73 (15), 4437-4451.
94. Latta, D. E.; Bachman, J. E.; Scherer, M. M. Fe Electron Transfer and Atom Exchange in Goethite: Influence of Al-Substitution and Anion Sorption. *Environmental Science & Technology* **2012,** 46 (19), 10614-10623.
95. Xu, W.; Hausner, D. B.; Harrington, R.; Lee, P. L.; Strongin, D. R.; Parise, J. B. Structural Water in Ferrihydrite and Constraints This Provides on Possible Structure Models. *American Mineralogist* **2011,** 96 (4), 513.
96. Hansel, C.; Learman, D.; Lentini, C.; Ekstrom, E. Effect of Adsorbed and Substituted Al on Fe (Ii)-Induced Mineralization Pathways of Ferrihydrite. *Geochim. Cosmochim. Acta* **2011,** 75 (16), 4653.
97. Adra, A.; Morin, G.; Ona-Nguema, G.; Menguy, N.; Maillot, F.; Casiot, C.; Bruneel, O.; Lebrun, S.; Juillot, F.; Brest, J. Arsenic Scavenging by Aluminum-Substituted Ferrihydrites in a Circumneutral Ph River Impacted by Acid Mine Drainage. *Environ. Sci. Technol.* **2013,** 47 (22), 12784.
98. Masue, Y.; Loeppert, R. H.; Kramer, T. A. Arsenate and Arsenite Adsorption and Desorption Behavior on Coprecipitated Aluminum:Iron Hydroxides. *Environmental Science & Technology* **2007,** 41 (3), 837-842.
99. Masue, Y.; Loeppert, R. H.; Kramer, T. A. Arsenate and Arsenite Adsorption and Desorption Behavior on Coprecipitated Aluminum: Iron Hydroxides. *Environ. Sci. Technol.* **2007,** 41 (3), 837.
100. Cismasu, A. C.; Michel, F. M.; Tcaciuc, A. P.; Tyliszczak, T.; Brown, G. E. Composition and Structural Aspects of Naturally Occurring Ferrihydrite. *C. R. Geosci.* **2011,** 343 (2), 210.

101. Cismasu, A. C.; Michel, F. M.; Stebbins, J. F.; Levard, C.; Brown, G. E. Properties of Impurity-Bearing Ferrihydrite I. Effects of Al Content and Precipitation Rate on the Structure of 2-Line Ferrihydrite. *Geochim. Cosmochim. Acta* **2012,** 92, 275.
102. Burton, E. D.; Bush, R. T.; Johnston, S. G.; Watling, K. M.; Hocking, R. K.; Sullivan, L. A.; Parker, G. K. Sorption of Arsenic (V) and Arsenic (Iii) to Schwertmannite. *Environ. Sci. Technol.* **2009,** 43 (24), 9202.
103. Jönsson, J.; Persson, P.; Sjöberg, S.; Lövgren, L. Schwertmannite Precipitated from Acid Mine Drainage: Phase Transformation, Sulphate Release and Surface Properties. *Appl. Geochem.* **2005,** 20 (1), 179.
104. Majzlan, J.; Myneni, S. C. B. Speciation of Iron and Sulfate in Acid Waters: Aqueous Clusters to Mineral Precipitates. *Environ. Sci. Technol.* **2005,** 39 (1), 188.
105. Regenspurg, S.; Peiffer, S. Arsenate and Chromate Incorporation in Schwertmannite. *Appl. Geochem.* **2005,** 20 (6), 1226.
106. Waychunas, G.; Xu, N.; Fuller, C.; Davis, J.; Bigham, J. Xas Study of Aso43– and Seo42– Substituted Schwertmannites. *Phys. B* **1995,** 208, 481.
107. Wilhelm Scherer, H. Sulfur in Soils. *Journal of Plant Nutrition and Soil Science* **2009,** 172 (3), 326-335.
108. Swedlund, P. J.; Webster, J. G.; Miskelly, G. M. Goethite Adsorption of Cu(Ii), Pb(Ii), Cd(Ii), and Zn(Ii) in the Presence of Sulfate: Properties of the Ternary Complex. *Geochimica et Cosmochimica Acta* **2009,** 73 (6), 1548-1562.
109. Ali, M. A.; Dzombak, D. A. Interactions of Copper, Organic Acids, and Sulfate in Goethite Suspensions. *Geochimica et Cosmochimica Acta* **1996,** 60 (24), 5045-5053.
110. Walter, M.; Arnold, T.; Reich, T.; Bernhard, G. Sorption of Uranium(Vi) onto Ferric Oxides in Sulfate-Rich Acid Waters. *Environmental Science & Technology* **2003,** 37 (13), 2898-2904.
111. Hoins, U.; Charlet, L.; Sticher, H. Ligand Effect on the Adsorption of Heavy Metals: The Sulfate — Cadmium — Goethite Case. *Water, Air, and Soil Pollution* **1993,** 68 (1), 241-255.
112. Geelhoed, J. S.; Hiemstra, T.; Van Riemsdijk, W. H. Phosphate and Sulfate Adsorption on Goethite: Single Anion and Competitive Adsorption. *Geochimica et Cosmochimica Acta* **1997,** 61 (12), 2389-2396.
113. Jain, A.; Loeppert, R. H. Effect of Competing Anions on the Adsorption of Arsenate and Arsenite by Ferrihydrite. *Journal of Environmental Quality* **2000,** 29, 1422-1430.
114. Wilkie, J. A.; Hering, J. G. Adsorption of Arsenic onto Hydrous Ferric Oxide: Effects of Adsorbate/Adsorbent Ratios and Co-Occurring Solutes. *Colloids and Surfaces A: Physicochemical and Engineering Aspects* **1996,** 107, 97-110.
115. Lefèvre, G.; Fédoroff, M. Sorption of Sulfate Ions onto Hematite Studied by Attenuated Total Reflection-Infrared Spectroscopy: Kinetics and Competition with Other Ions. *Physics and Chemistry of the Earth, Parts A/B/C* **2006,** 31 (10–14), 499-504.
116. Shipley, H. J.; Yean, S.; Kan, A. T.; Tomson, M. B. A Sorption Kinetics Model for Arsenic Adsorption to Magnetite Nanoparticles. *Environmental Science and Pollution Research* **2010,** 17 (5), 1053-1062.
117. Vaishya, R.; Gupta, S. Arsenic Removal from Groundwater by Iron Impregnated Sand. *J. Environ. Eng.* **2003,** 129 (1), 89.
118. Yang, Z.; Bertram, A. K.; Chou, K. C. Why Do Sulfuric Acid Coatings Influence the Ice Nucleation Properties of Mineral Dust Particles in the Atmosphere? *J. Phys. Chem. Lett.* **2011,** 2 (11), 1232.

119. Cziczo, D. J.; Froyd, K. D.; Gallavardin, S. J.; Moehler, O.; Benz, S.; Saathoff, H.; Murphy, D. M. Deactivation of Ice Nuclei Due to Atmospherically Relevant Surface Coatings. *Environ. Res. Lett.* **2009,** 4 (4), 044013.
120. Zhu, M.; Northrup, P.; Shi, C.; Billinge, S. J.; Sparks, D. L.; Waychunas, G. A. Structure of Sulfate Adsorption Complexes on Ferrihydrite. *Environ. Sci. Technol. Lett.* **2013,** 1 (1), 97.
121. Edgell, K. Usepa Method Study 37 Sw-846 Method 3050 Acid Digestion of Sediments, Sludges, and Soils [Microform] / Kenneth Edgell. U.S. Environmental Protection Agency, Environmental Monitoring Systems Laboratory: Cincinnati, Ohio, 1989.
122. Kubicki, J. D.; Kabengi, N.; Chrysochoou, M.; Bompoti, N. Density Functional Theory Modeling of Chromate Adsorption onto Ferrihydrite Nanoparticles. *Geochemical Transactions* **2018,** 19 (1), 8.
123. Goldberg, S.; Johnston, C. T. Mechanisms of Arsenic Adsorption on Amorphous Oxides Evaluated Using Macroscopic Measurements, Vibrational Spectroscopy, and Surface Complexation Modeling. *J. Colloid Interface Sci.* **2001,** 234 (1), 204.
124. Eggleston, C. M.; Hug, S.; Stumm, W.; Sulzberger, B.; Dos Santos Afonso, M. Surface Complexation of Sulfate by Hematite Surfaces: Ftir and Stm Observations. *Geochim. Cosmochim. Acta* **1998,** 62 (4), 585.
125. Parfitt, R. L.; Smart, R. S. C. The Mechanism of Sulfate Adsorption on Iron Oxides. *Soil Sci. Soc. Am. J.* **1978,** 42 (1), 48.
126. Anderson, M. A.; Rubin, A. J. Adsorption of Inorganics at Solid-Liquid Interfaces. *Soil Science* **1982,** 133 (4), 257-258.

APPENDICES

Appendix A

Appendix A.1. Oxyanion specific properties

Anion	**Ionic Radius (Å)** [1]	**Ionic Potential (Z/R)**	**Hydration Enthalpy (kJ/mol)** [2]	**Symmetry**[3]	**Structure**
Cl^-	1.81	0.55	-381	C_s	-
NO^{3-}	2.00	1.50	-314	D_{3h}	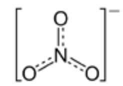
SO_4^{2-}	2.30	0.01	-1059	C_{2V}	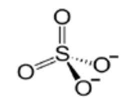
PO_4^{3-}	2.38	0.84	-2921	T_d	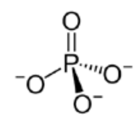
AsO_4^{3-}	2.48	1.21	-3033	T_d	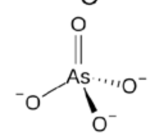

[1] *Marcus, Y. Ions and Their Properties. In Ions in Solution and their Solvation, John Wiley & Sons, Inc: 2015; 10-62.*

[2] *Smith, D. W. Ionic hydration enthalpies. Journal of Chemical Education 1977, 54 (9), 540.*

Marcus, Y. Mutual Effects of Ions and Solvents. In Ions in Solution and their Solvation, John Wiley & Sons, Inc: 2015; 156-192.

Engel, T. Quantum Chemistry & Spectroscopy. New York: Pearson Education, 2006

Arai, Y.; Sparks, D. L. Atr–Ftir Spectroscopic Investigation on Phosphate Adsorption Mechanisms at the Ferrihydrite–Water Interface. Journal of Colloid and Interface Science ***2001,*** *241 (2), 317-326.*

Appendix B

Appendix B.2. Representative X-ray Diffraction Pattern for Ferrihydrite

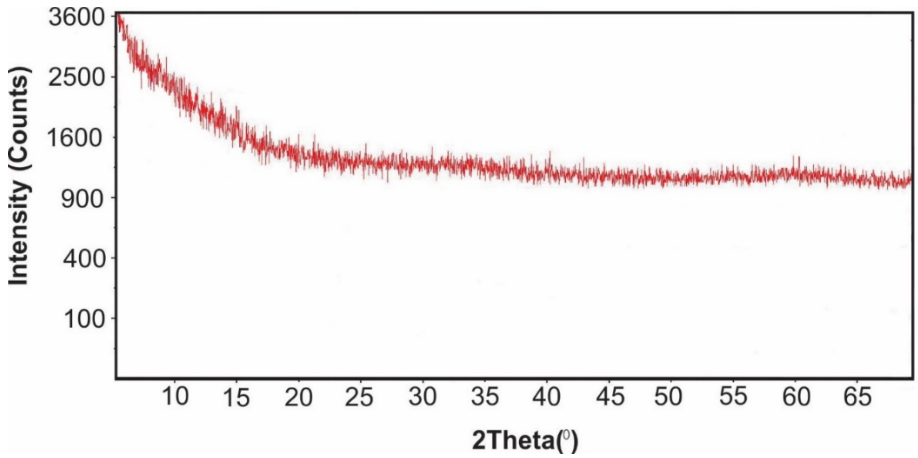

Appendix B.3. Representative High-Resolution Transmission Electron Micrograph of the Ferrihydrite Sample

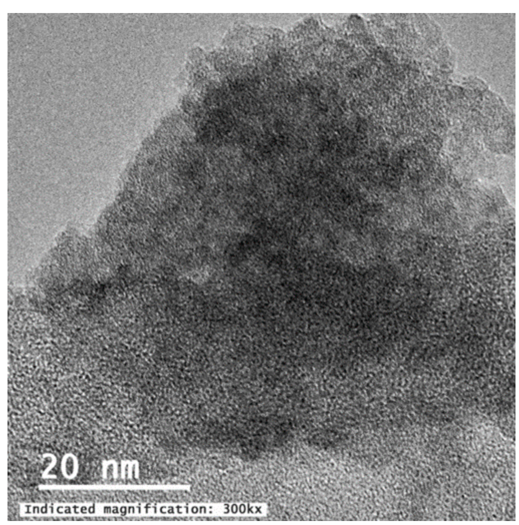

Appendix B.4. Instrumentation and Basic Operational Procedure for the Flow Microcalorimeter

The flow microcalorimetry used in this work is comprised of microcolumn assembly with a sample holder in which a solid sample is packed. A solution of interest is injected in the column and flows over the micro column containing the packed solid, while the flow rate is controlled between 0.30 to 0.350 ml min1- until the thermal equilibrium is obtained evidenced by a steady baseline. As the input solution is switched to another solution with different composition (e.g., pH, ionic strength or concentration), the change in temperature resulting from either heat produced or consumed as the reacting solute interacts with the solid surface is recorded by a pair of thermistors, one upstream and one downstream from the sample holder, form one half of an electronic bridge. The calorimetrical signal, then, is displayed graphically and recorded as a function of time as the peak of reaction returns back to the pre-experiment baseline indicating the end of reaction. The flow rate-averaged peak areas are acquired by integrating the calorimetric peak. The heats of reactions (Q in mJ/mg solid) is calculated by converting the peak area to energy (Joules) using peaks of known energy input generated from a calibrating resistor located within the flow stream inside the micro-column (Appendix A.4 a and b).

Appendix B.5. a) Peaks Obtained From a Series of Heat Pulses, and b) The Associated Calibration Curve.

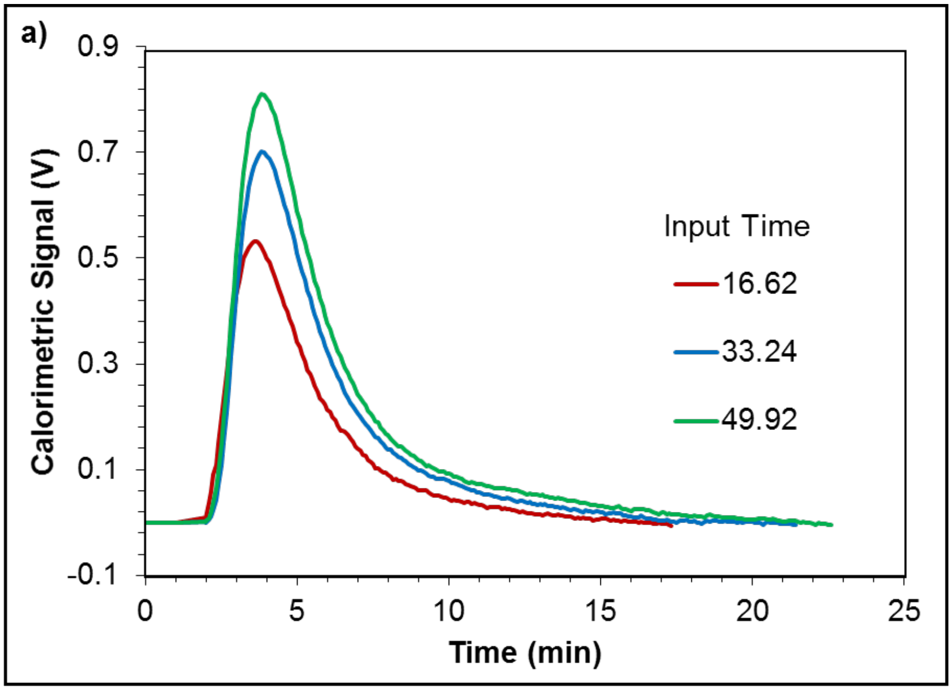

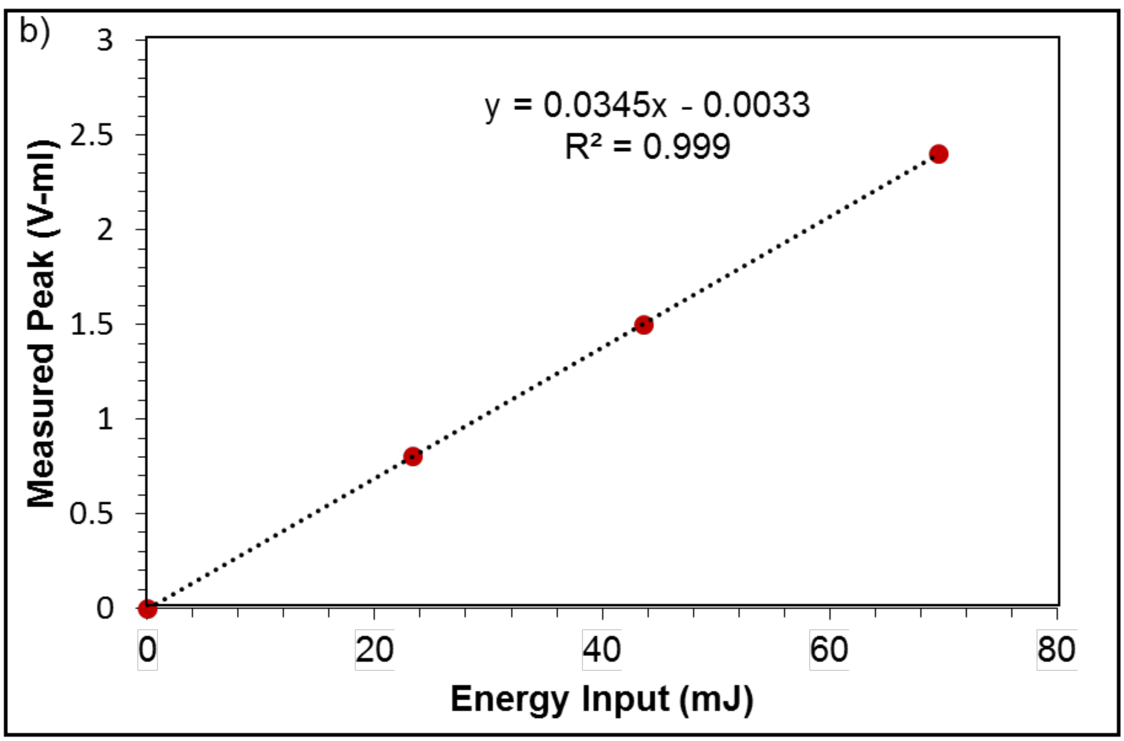

Appendix C

Appendix C.1. Representative X-ray Diffraction Pattern for Different Aluminum Ferrihydrite

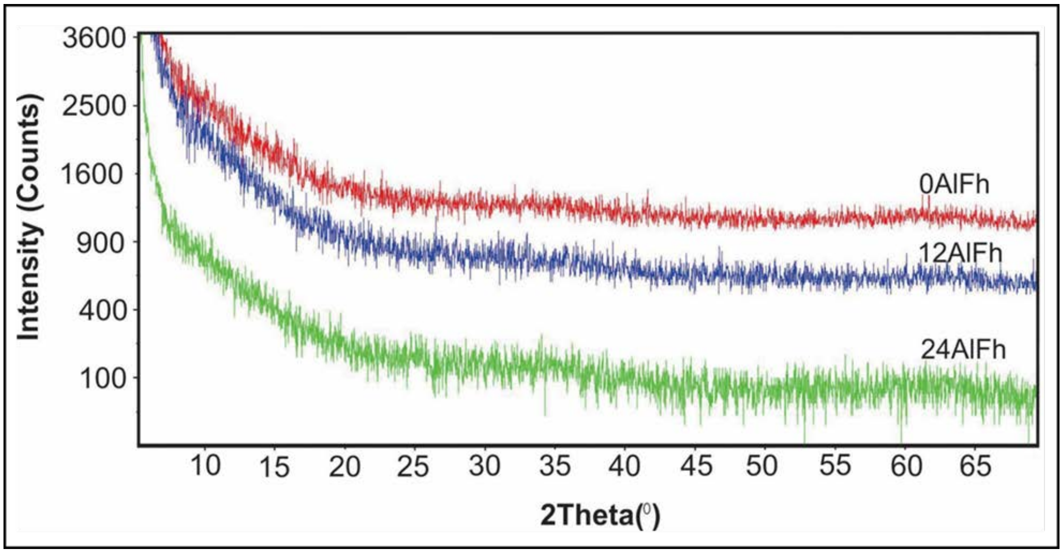

Appendix C.2. Zeta Potential Data for Ferrihydrite (0AlFh), and Al-ferrihydrite (12AlFh and 24AlFh)

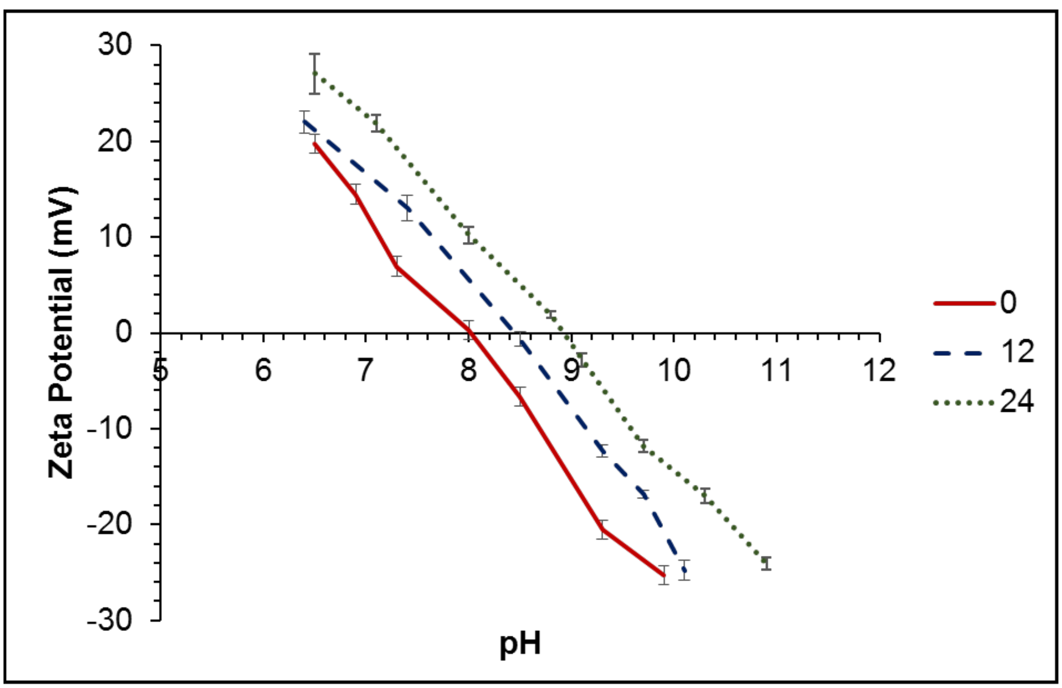

Appendix C.3. Transmission Electron Micrographs and Energy Dispersive X-ray Spectroscopy Analysis of Different Aluminum Ferrihydrite

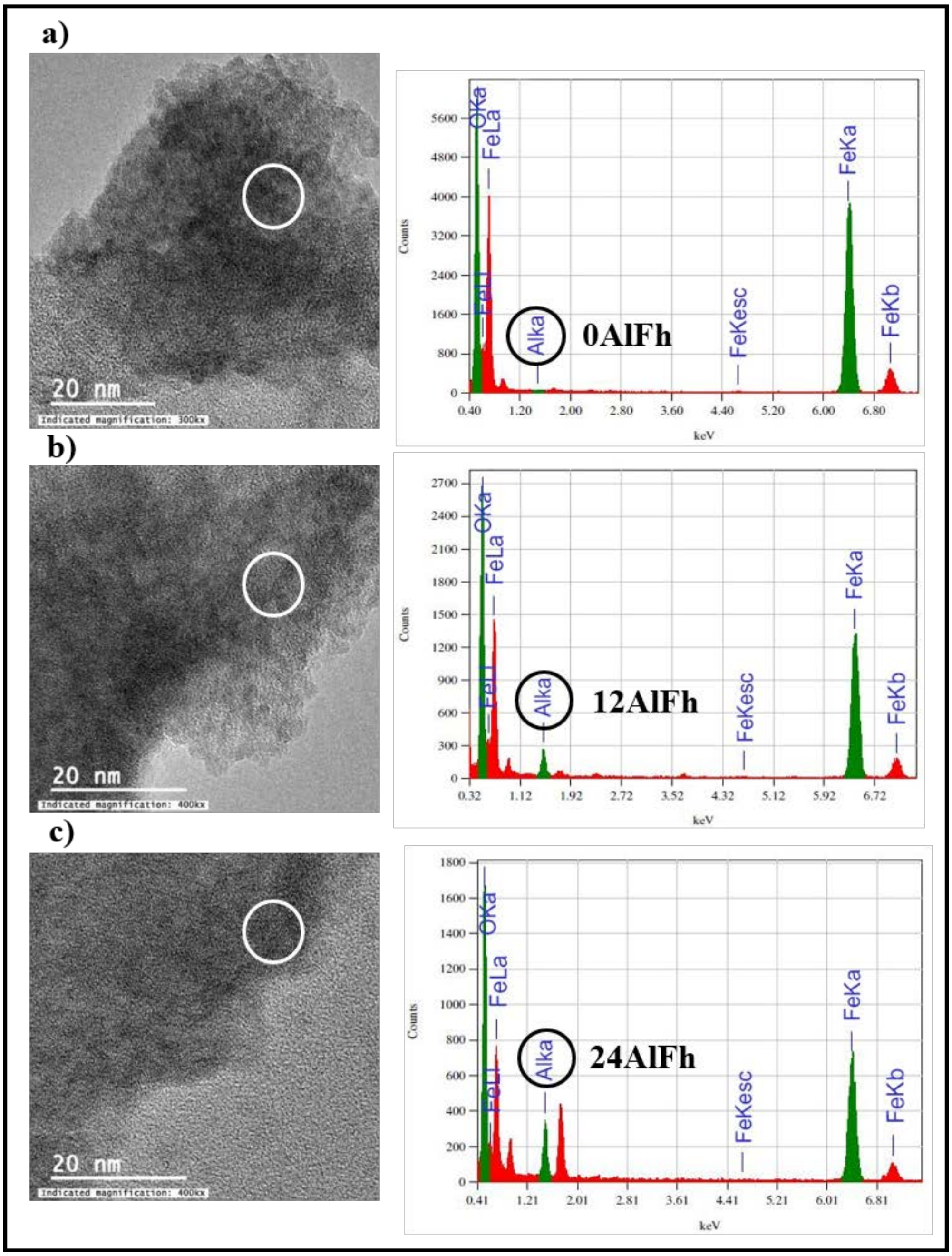

Appendix C.4. The Q_{exch} of C/N (mJ/mg) of Various AlFh at pH 5.6 and pH 3